Am J Physiol Gastrointest Liver Physiol 311: G396–G411, 2016.
First published May 26, 2016; doi:10.1152/ajpgi.00027.2016.

Yes-associated protein impacts adherens junction assembly through regulating actin cytoskeleton organization

Haibo Bai,[1]* Qingfeng Zhu,[2]* Alexandra Surcel,[3] Tianzhi Luo,[3] Yixin Ren,[3] Bin Guan,[1] Ying Liu,[1] Nan Wu,[6] Nora Eve Joseph,[5] Tian -Li Wang,[1] Nailing Zhang,[4] Duojia Pan,[4] Gianfranco Alpini,[6] Douglas N. Robinson,[3] and Robert A. Anders[1]

[1]*Department of Pathology, Johns Hopkins University School of Medicine, Baltimore, Maryland;* [2]*Institute of Biomedical Sciences (IBS), Fudan University, Shanghai, People's Republic of China; and Department of Pathology, Johns Hopkins University School of Medicine, Baltimore, Maryland;* [3]*Department of Cell Biology, Johns Hopkins School of Medicine, Baltimore, Maryland;* [4]*Department of Molecular Biology and Genetics, Howard Hughes Medical Institute, Johns Hopkins School of Medicine, Baltimore, Maryland;* [5]*Department of Pathology, University of Chicago, Chicago, Illinois; and* [6]*Research, Central Texas Veterans Health Care System, Temple, Texas; Department of Medicine, Division of Gastroenterology, Texas A&M Health Science Center College of Medicine, Temple, Texas; and Baylor Scott & White Health Digestive Disease Research Center, Temple, Texas*

Submitted 5 February 2016; accepted in final form 11 May 2016

Bai H, Zhu Q, Surcel A, Luo T, Ren Y, Guan B, Liu Y, Wu N, Joseph NE, Wang TL, Zhang N, Pan D, Alpini G, Robinson DN, Anders RA. Yes-associated protein impacts adherens junction assembly through regulating actin cytoskeleton organization. *Am J Physiol Gastrointest Liver Physiol* 311: G396–G411, 2016. First published May 26, 2016; doi:10.1152/ajpgi.00027.2016.—The Hippo pathway effector Yes-associated protein (YAP) regulates liver size by promoting cell proliferation and inhibiting apoptosis. However, recent in vivo studies suggest that YAP has important cellular functions other than controlling proliferation and apoptosis. Transgenic YAP expression in mouse hepatocytes results in severe jaundice. A possible explanation for the jaundice could be defects in adherens junctions that prevent bile from leaking into the blood stream. Indeed, immunostaining of E-cadherin and electron microscopic examination of bile canaliculi of *Yap* transgenic livers revealed abnormal adherens junction structures. Using primary hepatocytes from *Yap* transgenic livers and *Yap* knockout livers, we found that YAP antagonizes E-cadherin-mediated cell-cell junction assembly by regulating the cellular actin architecture, including its mechanical properties (elasticity and cortical tension). Mechanistically, we found that YAP promoted contractile actin structure formation by upregulating nonmuscle myosin light chain expression and cellular ATP generation. Thus, by modulating actomyosin organization, YAP may influence many actomyosin-dependent cellular characteristics, including adhesion, membrane protrusion, spreading, morphology, and cortical tension and elasticity, which in turn determine cell differentiation and tissue morphogenesis.

actin cytoskeleton; YAP; adherens junctions

YES-ASSOCIATED PROTEIN (YAP), a transcription coactivator, is negatively regulated by the Hippo tumor suppressor pathway (26, 48, 66). In mammalian tissues, Hippo signaling is generally thought to act through YAP to regulate cell proliferation and apoptosis. However, in tissue-specific gain-of-function or loss-of-function genetically modified mouse models, YAP is required for tissue morphogenesis in multiple organs independent of proliferation or apoptosis. For example, increasing YAP activity by ablating its negative regulators *Mst1* and *Mst2* leads to significantly smaller pancreases due to postnatal differentiation of acinar cells into duct-like cells (23). In mouse kidney, loss of *Yap* leads to defects in nephron formation and morphogenesis during renal development, independent of major changes in apoptosis or proliferation (50). In mouse livers, YAP hyperactivation due to *Nf2* deficiency results in increased biliary epithelial cell differentiation while *Yap* deficiency leads to bile duct paucity (65). Collectively, these studies suggest functions of YAP that extend beyond simple control of proliferation and apoptosis and that implicate other systems that regulate tissue morphology.

The actin cytoskeleton is an important subcellular machinery that is involved in essentially all aspects of cell physiology, including controlling and maintaining cell morphology, regulating cell motility, governing cell proliferation, and mediating cell communication and signal transduction (49). The organization of the actin cytoskeleton is significantly impacted by the coordinated assembly, contraction, and relaxation of actin-myosin meshwork (58). Myosin II-generated tension is a primary force of cellular contractility and is activated by the phosphorylation of the myosin regulatory light chain. This light chain phosphorylation generally occurs on Ser19, either alone or in combination with Thr18, and facilitates the interactions between the myosin II motor and actin filaments. Myosin light chain kinase (57) and Rho-associated kinase (ROCK) (47) are essential regulators of myosin light chain phosphorylation.

Of the different mechanisms that mediate E-cadherin junction dynamics, the actin cytoskeleton is a chief determinant of junction stability (32). In cultured cells, mature stable and nascent dynamic E-cadherin junctions are accompanied by distinct actin cytoskeletal structures. In fully formed epithelial sheets with mature E-cadherin junctions, a cortical belt of actin cables underlies a continuous E-cadherin junctional belt. During the early stages of junction formation, as well as during junction disassembly, radial actin cables connect cell-cell contacts to circumferential actin rings (34, 60, 64). While the mechanisms of transformation between these two junction-accompanied actin networks remain poorly understood, the make-up of the circumferential actin rings has been extensively characterized. Nonmuscle myosin II localizes to the circumferential actin rings, suggesting that they are under tension (60)

* H. Bai and Q. Zhu contributed equally to this work.

Address for reprint requests and other correspondence: R. A. Anders, Dept. of Pathology, Johns Hopkins Univ. School of Medicine, Baltimore, MD (e-mail: rander54@jhmi.edu).

and that this myosin II-generated tension is a major mode of regulating adherens junction assembly, maintenance, and disassembly (15, 33, 54).

In this study, we describe the role of YAP in regulating adherens junction organization in hepatocytes. We first observed that ectopic expression of YAP in hepatocytes led to abnormal adherens junction assembly in vivo. Further exploring YAP's role in adherens junction assembly with primary hepatocytes cultured in vitro, we found that YAP antagonized E-cadherin junction assembly by regulating actin cytoskeleton architecture. Finally, we identified that YAP promotes contractile actin ring formation by combined upregulation of nonmuscle myosin light chain expression and cellular ATP production.

MATERIALS AND METHODS

Animals. All animals were housed at The Johns Hopkins University animal facility and handled according to National Institutes of Health guidelines. The animal studies were approved by The Johns Hopkins University Institutional Animal Care and Use Committee. The liver-specific *Yap* transgenic mice (*ApoE/rtTA-Yap*), which overexpresses YAP, and the *Yap* knockout mice (*Mx1-Cre; Yap$^{flox/flox}$*) have been described (18, 65). The liver-specific Yap and TEAD2 dominant-negative transgenic mice (ApoE/rtTA-Yap/TEAD2 DN) were described previously (44). To avoid potential variation related to gender, all experiments were performed in male mice with paternal inheritance of *Mx1-Cre*. Activation of *Mx1* promoter was induced via three intraperitoneal injections of 600 μg polyIC (P1530; Sigma) every other day to 5-wk-old mice as previously described (65). One week after polyIC injection, bile duct ligation (BDL) was performed as described previously (24) with *Mx1-Cre; Yap$^{flox/flox}$* mice and their wild-type (WT) littermates *Yap$^{flox/flox}$* mice. The livers were harvested 5 days post-BDL. Serum levels of total bilirubin were measured using a kit from Biotron diagnostic according to the manufacturer's protocol.

Immunohistochemistry staining. Mouse livers were fixed for 48 h in 10% neutral buffered formalin solution (Sigma) embedded in paraffin and sectioned at 5 μm. Immunohistochemical staining was performed according to the protocols provided by the manufacturers of the antibodies. The primary antibody used was E-cadherin (CST; no. 3195; 1/100). The secondary antibody used was Envision anti-rabbit (DAKO; no. K4002).

Transmission electron microscopy. Yap transgenic (*Yap*-Tg) mice and their littermate controls were fed with doxycycline (Dox)-containing water for 2 wk before harvest. *Mx1-Cre; Yap$^{flox/flox}$* (*Yap*-KO) mice and their littermate controls were injected with polyIC 2 wk before harvest. Freshly harvested livers were cut into 1- to 2-mm^3 pieces and fixed using 3% glutaraldehyde in Millonig's phosphate buffer (0.1 M, pH 7.2) at 4°C overnight. The liver tissues were then washed three times and maintained with Millonig's phosphate buffer (0.1 M, pH 7.2) at 4°C. The transmission electron microscopy of WT, *Yap*-Tg, and *Yap*-KO livers was performed at the Electron Microscope facility of University of Chicago and the Microscopy Imaging Center, University of Vermont.

Protein lysate and Western blot analysis. Mouse livers or primary hepatocytes were lysed in RIPA buffer. The proteins were separated on SDS-polyacrylamide gels and transferred onto nitrocellulose membranes (Bio-Rad). The blots were probed with antibodies against E-cadherin (no. 3195; 1/1000; CST), phospho-myosin light chain 2 (Ser19) antibody (no. 3671; 1/1,000; CST), and myosin light chain 2 (D18E2) rabbit mAb (no. 8505; 1/1,000; CST) and normalized by GAPDH (no. 9385; 1/5,000; Abcam). Signals were detected and quantified on the LI-COR Infrared Imaging system.

Nuclear/cytoplasmic fractionation. Nuclear/cytoplasmic fractionation was performed essentially as described in (13). Briefly, *day 1* hepatocytes harvested from 10-cm culture dishes were resuspended with five times of the volume of pellet with buffer-A (10 mM HEPES, pH 7.9, 1.5 mM $MgCl_2$, 10 mM KCl, 0.5 mM DTT, and 1× protease inhibitor) and incubated on ice for 15 min, followed by homogenization with a tissue grinder. Cell lysis was checked by trypan blue staining of the nucleus after every 20 strokes. The cell lysate was centrifuged at 1,000 *g* for 5 min to separate the nuclei in the pellet fraction and the cytoplasm in the supernatant fraction. The nuclear fraction was washed two times with buffer-A and centrifuged (1,000 *g* for 5 min each) and resuspended with buffer-A to a similar volume as the cytoplasmic fraction and sonicated. Protein concentrations were measured with the nuclear and cytoplasmic extracts. Five micrograms of protein from each fraction were immunoblotted for YAP, GAPDH (cytoplasmic fraction marker), and histone H3 (nuclear fraction marker).

Primary hepatocyte isolation and culture. Hepatocytes were isolated by two-step collagenase perfusion (41). Isolated hepatocytes were cultured in a collagen-coated cell culture dish and in culture medium as described previously (41). To induce YAP expression in the hepatocytes from *Yap*-Tg mice, 1 μg/ml Dox was added to the culture medium the morning following isolation. The time point when the Dox was added to the cell culture was considered *time 0*. ML7 (no. 4310; Toris Bioscience), a selective myosin light chain kinase inhibitor, and Y27632 (no. 1254; Toris Bioscience), a selective Rho-associated kinase inhibitor, were used to inhibit myosin light chain phosphorylation, which in turn inhibit nonmuscle myosin II activity (7, 55). ML-7 (5 μM) and Y27632 (25 μM) were added to culture medium at *time 0* and incubated for 24 h preceding fixation. If not specified, primary hepatocytes were cultured in high glucose medium (4.5 g/l). In low glucose medium, the glucose concentration was 1 g/l.

Cell lines and treatment. The mouse hepatocytes cell line AML12 (WT) from ATCC was cultured with DMEM/F-12 medium (GIBCO) supplemented with insulin, transferrin, selenium (ITS; GIBCO), dexamethasone (DEX) (40 ng/ml; Sigma), and 100 U/ml penicillin and 100 μg/ml streptomycin, in a humidified atmosphere containing 5% CO_2 at 37°C. Lentiviral plasmids containing shRNAs (Open Biosystems) against mouse Yap, shRNA against eGFP or Yap gene coding sequence were used to construct AML12-Yap-Knockdown (KD), AML12-Control (CTRL), and AML12-Yap-overexpression (OE). Expression was confirmed by Western analysis using anti-YAP antibodies.

Immunofluorescence staining. At 24 h, primary hepatocytes cultured in 24-well plates were fixed with 10% buffered formalin for 15 min. After being washed with TBST (137 mM sodium chloride, 20 mM Tris, and 0.05% Tween-20, pH 7.6), cells were permeabilized in 0.5% Triton X-100 for 15 min at room temperature followed by blocking in TBST containing 5% bovine serum albumin (blocking buffer) for 10 min at 37°C. Samples were incubated with primary antibodies diluted in blocking buffer for 60 min at 37°C. Cells were washed and incubated for 30 min with Alexa dye-conjugated secondary antibodies, followed by washing and mounting with circular cover slips using ProLong antifade reagent (Life Technologies). The primary antibodies used in this study were ZO-1 (no. 61–7300; Thermo Fisher; 1/25), E-cadherin (#13–1900; Life Technologies; 1/100), and rhodamine-phalloidin (no. R415; Life Technologies; 1/100). The secondary antibodies used were goat anti-rat (A11006; Life Technologies; 1/100) and goat anti-rabbit (A11034; Life Technologies; 1/100). Labeled primary hepatocytes were imaged using a Nikon Eclipse Ti fluorescence microscope. Snap-frozen tissues embedded in O.C.T. were cut into 8-μm sections, which were used for immunofluorescent staining according to the protocols provided by the manufacturer of the ZO-1 antibody (no. 61–7300; Thermo Fisher; 1/25). The secondary antibody used was goat anti-rabbit (A11034; Life Technologies; 1/100). Immunofluorescent images were visualized using Leica AF 6000 Modular 146 Systems (Leica Biosystems, Newcastle, UK). Presented images are representative of at least three independent experiments.

Live cell microscopy and lamella quantification. Primary hepatocytes were isolated and plated onto a collagen-coated, 35-mm dish and cultured for 24 h before imaging. The time-lapse images were acquired with an inverted microscope (Eclipse Ti; Nikon) equipped with a heated chamber and CO_2 controlling unit (Tokit). Time-lapse sequences were collected at seven stage-position sites with consecutive phase contrast images every 10 min for 48 h. Lamellae were counted from three randomly selected stage-position sites for each mouse.

Cortical elasticity and cortical tension measurements. The deformability of primary hepatocytes was measured using micropipette aspiration as described previously (20, 51). In short, aspiration pressure was applied to the surface of newly isolated hepatocytes using glass pipettes with an inner radius of ~8–10 μm. Cells were imaged using an Olympus IX81 microscope with a ×40 (NA 1.3) objective and a ×1.6 optovar. Images were acquired using MetaMorph Software (Molecular Devices). DIC (10-ms exposure) images were collected at 5-s intervals. The length of the cell tether inside of the pipette (L_p) and the radius of the pipette (R_p) were measured using ImageJ software (http://imagej.nih.gov/ij/). The measured L_p/R_p was plotted vs. the applied pressure (ΔP), and the elastic moduli were calculated from the slopes of the linear fits to these data (30, 51). For cortical tension measurements, the pressure was applied to the cell cortex with a glass micropipette (3- to 4-μm radius) to the equilibrium pressure (ΔP), where the L_p was equal to R_p and calculated as previously described (16, 36). Ten to 30 cells were aspirated for each condition.

Physical model of YAP-regulated cell-cell adhesion. Epithelial cells undergoing shape change may adopt different geometric configurations depending in part, on actomyosin contractility and cell-cell adhesion. Similar to the cases of cell-substrate interaction (5, 56, 61), the energy of the system consisting of quasi two-dimensional epithelial cells, E_{total}, has the simple form of

$$E_{total} = E_{bending} + E_{dilation} - E_{adhesion} \quad (1)$$

where $E_{bending}$, $E_{dilation}$, and $E_{adhesion}$, are the bending energy associated with curvature change, dilation energy of the actin cortex, and adhesion energy, respectively. For a layer of epithelial cells, the change of dilation energy is driven by the tension per unit area due to the varying of actomyosin contractility. For two configurations with different total energy, the configuration with smaller E_{total} is more energetically favorable, meaning that the system tends to evolve from the high energy configuration to the low energy configuration. As the bending energy is relatively small, the evolution of the system energy is mainly driven by the competition between the cell-cell adhesion and actomyosin-contractility dominated tension.

The change of the system energy for different configurations can be calculated by varying the major geometrical parameters once the dilation and cell-cell adhesion energy are quantitatively defined. Additionally, the geometry of cell shape can be numerically determined provided that the thickness of the epithelial cells does not change and that the cellular volume is almost constant. Due to the sixfold symmetry of a simplified model cell (see Fig. 5*A*), the geometrical parameters include l, α, and β, with the geometrical constraint $\alpha + \beta = \pi/3$. When $\alpha = \pi/3$ and $\beta = 0$, the cell has a circular cross section and no cell-cell adhesion (see Fig. 5*F*, *right*). For the case of $\alpha = 0$ and $\beta = \pi/3$, the cross section is a perfect hexagon and cell-cell adhesion is maximized (see Fig. 5*F*, *left*). The bending energy is determined by

$$E_{bending} = 6\left[\frac{1}{2}k_{bending}\left(\frac{1}{l} - \frac{1}{r_0}\right)^2 \widehat{BC}\cdot h + \frac{1}{2}k_{bending}\left(-\frac{1}{r_0}\right)\overline{AB}\cdot h\right]. \quad (2)$$

The term $k_{bending}$ (~400 $k_BT/\mu m^2$; Ref. 17) is the bending modulus, r_0 is the radius (~19 μm), and h is the thickness of the epithelial cells (5 μm). The dilation energy is

$$E_{dilation} = \sigma \cdot \Delta A/A_0 \cdot A_{lateral}. \quad (3)$$

The term σ is the tension for the cell cortex and was determined by converting the measured Young's modulus (see Fig. 4*C*), while assuming the cortex is ~0.3-μm thick. A_0 is the surface area of an epithelial cell with a circular cross section of radius r_0 and has the value of $2\pi_0^2 + 2\pi_0 h$. $A_{lateral}$ is the lateral surface area and reads $A_{lateral} = 6h\{1\alpha + 2l\sin[(\pi/3 - \alpha)/2]\}$. ΔA is the area difference between a cell with noncircular cross section A and A_0. A_0 can be determined by $A = 6l^2\{\alpha + 0.5\sin[(\pi/3 - \alpha)/2]\} + A_{lateral}$. Based on the fluorescence images for the different cells (see Fig. 2), we assume that the concentrations of myosin and actin only have significant changes on the lateral surface, not on the basal and apical surfaces. The adhesion energy is

$$E_{adhesion} = 6\overline{AB}\cdot h\cdot(\rho\varepsilon - \gamma), \quad (4)$$

where ρ is the cadherin bond density at the cell-cell interface, ε is the bond energy of cadherin-cadherin complexes, and γ is the interfacial energy between the cell surface and the culture medium. Here, the product ρε has a value of 7,000 $k_BT/\mu m^2$ for WT cells (29), which is based on the estimation of $\rho = 350$ molecules/μm^2 (1) and $\varepsilon = 20$ k_BT (12, 35). Meanwhile, γ is taken as 0 for simplicity. For the same reason, we also neglect the surface energy change associated with the area change of basal and apical surfaces.

Hanging drop adhesion assay. The hanging drop adhesion assay was performed as described with some modifications (45). Freshly isolated primary hepatocytes cells were resuspended at 1×10^5 cells/ml. Twenty-microliter drops of cell suspension were pipetted onto the inner surface of 10-cm Petri dish lids, and dishes were filled with 10 ml of PBS to prevent evaporation. At each time point, the lid was inverted and coverslips were placed over the drops. Three random 10× fields at the area with highest cell concentration from each drop were imaged and photographed using a Nikon Eclipse TS100 microscope, and numbers and sizes of clusters were determined. Data from each field were combined to determine the overall fraction of cells in each cluster size. The experiments were repeated independently from three animals of each genotype.

Quantitative real-time PCR. Day 1 hepatocyte RNA was extracted using PureLink RNA extraction kit (Thermo Fisher). RNA was reverse-transcribed with random primers using iScript cDNA synthesis kit (Bio-Rad). Real-time quantitative PCR (qPCR) was performed using the Quantitect SYBR Green PCR kit (Thermo Fisher) on a ViiA7 Realtime PCR System (Applied Biosystems). qPCR was done in triplicate, using histone H2A.Z as a housekeeping control. Relative differences in the expression of the candidate genes in control and mutant livers were determined using the $^{2-\Delta\Delta}C_t$ method. The primer sequences used are available on request.

Intracellular ATP quantification. For newly isolated primary hepatocytes, 4×10^4 cells were suspended in 50 μL TE buffer (0.1 M Tris·HCl and 4 mM EDTA pH 7.5), boiled for 7 min, and centrifuged at 14,000 rpm for 2 min. Ten microliters of the supernatant were used for ATP quantification. For cultured primary hepatocytes, 1×10^4 cells were seeded into each well of a 96-well plate. On *day 1*, the cells were suspended in 50 μl TE buffer, boiled for 7 min, and centrifuged at 14,000 rpm for 2 min. The relative live cell numbers were determined by manually counting five random ×200 fields under the microscope of DAPI-stained samples. ATP amounts were measured according to the manufacturer's protocol from the ATP determination kit (no. A22066; Thermo Fisher).

RESULTS

YAP antagonizes hepatocyte adherens junction stability in mouse liver. Transgenic YAP overexpression in mouse hepatocytes (*Yap*-Tg liver) promotes cell proliferation, leading to liver overgrowth (18). In addition to these results, we also observed severe jaundice in the *Yap*-Tg mice after a 2-wk induction of YAP overexpression by Dox feeding. Measure-

ment of the total serum bilirubin revealed significantly higher levels in *Yap*-Tg mice (total serum bilirubin, 17.0 ± 4.3 mg/dl), compared with 2-wk Dox-fed WT littermates (total serum bilirubin, 0.4 ± 0.2 mg/dl) (Fig. 1*A*). Two weeks after induction of liver-specific *Yap* deficiency by injection of *polyIC* to *Mx1-Cre; Yap*$^{flox/flox}$ knockout (*Yap*-KO) mice, serum total bilirubin levels (0.7 ± 0.3 mg/dl) were unchanged.

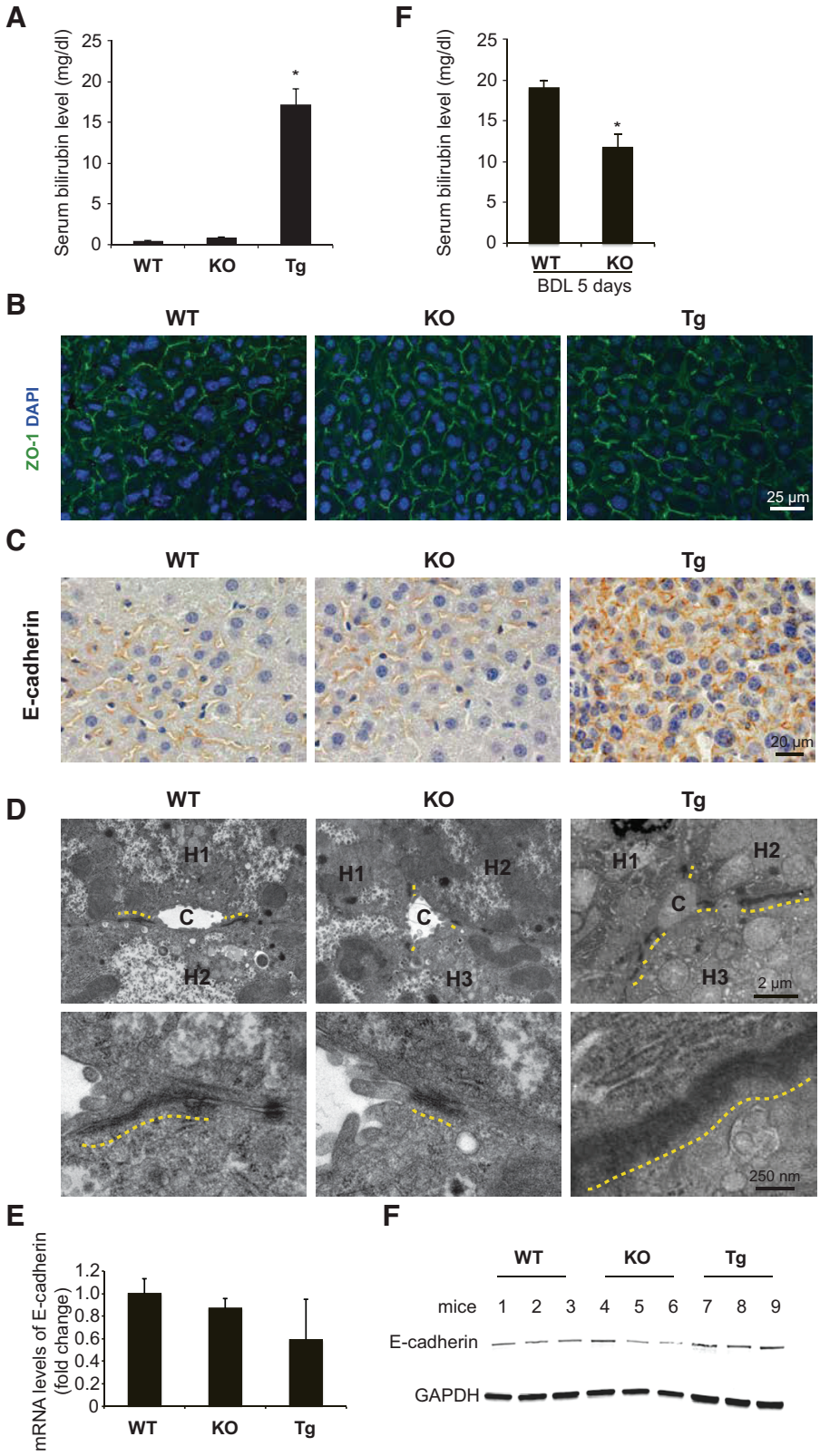

Fig. 1. Yes-associated protein (YAP) antagonizes hepatocyte adherens junction stability in mouse livers. *A*: serum total bilirubin levels of wild type (WT) mice, *Yap*-KO (KO) mice, and *Yap*-Tg (Tg) mice. Bars represent mean ± SE (n = 3 mice from each genotype). *$P < 0.05$, compared with WT by one-way ANOVA and Fisher's least significant difference posttest. *B*: ZO-1 staining of WT, *Yap*-KO, and *Yap*-Tg livers. *C*: E-cadherin staining of WT, *Yap*-KO, and *Yap*-Tg livers. Note more E-cadherin staining on the hepatocyte membrane of *Yap*-Tg livers. *D*: transmission electron microscopy images of WT, *Yap*-KO, and *Yap*-Tg livers showed the length of adherens junctions (indicated by yellow dash lines) surrounding bile canaliculi positively correlated with YAP levels. The electron dense zones demarcating the adherens junctions in *Yap*-Tg livers extended for a longer distance along the membrane and penetrated further into the cytoplasm. H, hepatocyte; C, bile canaliculi. *E*: E-cadherin mRNA levels in WT, *Yap*-KO, and *Yap*-Tg livers. Bars represent mean ± SE (n = 3 mice from each genotype). *F*: E-cadherin protein levels WT, *Yap*-KO, and *Yap*-Tg livers. *G*: serum total bilirubin levels of WT and KO mice 5 days after BDL. Bars represent mean ± SE (n = 5 mice from each genotype). *$P < 0.05$, compared with WT by unpaired t-test.

Because the *Yap* transgene was only expressed in hepatocytes under the *ApoE* promoter and the biliary system was histologically normal in the 2-wk Dox-fed *Yap*-Tg mice (data not shown), we reasoned that the jaundice may be due to dysregulated tight junctions and adherens junctions, which function to seal the bile canaliculi to prevent bile from flowing into the plasma. ZO-1 staining of tight junctions showed no significant changes among WT, *Yap*-KO, and *Yap*-Tg livers (Fig. 1*B*). However, E-cadherin staining of WT, *Yap*-KO, and *Yap*-Tg livers revealed more extensive E-cadherin distribution along the *Yap*-Tg hepatocyte cortex, compared with WT and *Yap*-KO hepatocytes (Fig. 1*C*). Consistently, electron microscopy showed that the expansion of adherens junctions surrounding bile canaliculi positively correlated with YAP protein levels in WT, *Yap*-KO, and *Yap*-Tg livers. More importantly, the morphology of the adherens junctions was abnormal in the *Yap*-Tg liver with a more diffuse appearance compared with WT or *Yap*-KO livers (Fig. 1*D*). However, no differences in E-cadherin mRNA or protein levels were detected among WT, *Yap*-KO, and *Yap*-Tg livers (Fig. 1, *E* and *F*).

Two major possibilities could account for the relationship between YAP expression and adherens junction formation. First, YAP may promote adherens junction formation, leading to their expansion along the *Yap*-Tg hepatocyte surface. Alternatively, YAP may destabilize adherens junction formation, resulting in diffuse, defective adherens junction structures. These defective adherens junctions would in turn lead to bile escaping into blood stream. The tissue may then attempt to compensate by accumulating more E-cadherin to the hepatocyte cortex in the *Yap*-Tg livers. In the first scenario, we expect that the *Yap* KO livers would have less stable adherens junctions. In the second scenario, we expect that *Yap* KO livers would have more stable adherens junctions. To test these hypotheses, we induced blood-biliary barrier leakage by performing the common BDL with *Yap* KO and WT mice (24). The *Yap* KO mice showed significantly lower serum bilirubin levels (11.8 ± 1.69 mg/dl) compared with their WT littermates (19.1 ± 0.9 mg/dl) (Fig. 1*G*). These data suggest that adherens junctions of *Yap*-KO hepatocytes were more stable than those of WT hepatocytes. Therefore, we concluded that YAP likely functions to antagonize adherens junction stability in hepatocytes. To test this idea and to discern the mechanisms underlying this antagonism, we turned to isolated primary hepatocytes.

YAP antagonizes E-cadherin junction assembly in primary hepatocytes. To investigate how YAP expression levels affect adherens junction formation, we employed primary hepatocytes because of their ability to form E-cadherin junctions in culture (14). *Yap*-Tg primary hepatocytes were isolated from *Yap*-Tg livers without pre-Dox feeding. The day after isolation (*day 0*), 1 μg Dox was added to the culture medium to induce transgenic YAP expression. On *day 1* (24 h later), the cells were fixed and stained for E-cadherin. By inducing Yap expression for only 24 h, the phenotypes observed in *Yap*-Tg hepatocytes should reflect a fairly acute impact of changing YAP levels, rather than the long-term adaptation by the cells to new levels of Yap expression. *Yap*-KO hepatocytes were isolated from 2-wk-post *polyIC*-injected *Mx1-Cre; Yap*$^{flox/flox}$ livers, which did not show histological abnormalities in vivo (4), and the WT hepatocytes were isolated from the WT littermates of the *Yap*-KO mice. Yap KO and WT hepatocytes were also harvested on *day 1*. Significant increases of YAP protein levels in *Yap*-Tg hepatocytes and YAP protein deletion in *Yap*-KO hepatocytes were confirmed by Western analysis of whole cell lysates (Fig. 2*A*). Without manipulation of YAP's subcellular distribution regulators (3, 18), the subcellular distribution patterns of YAP were maintained in the *Yap*-Tg hepatocytes in a similar manner to that of WT hepatocytes but with increased protein levels in each compartment (Fig. 2*A*). Thus the increased Yap activity in the *Yap*-Tg hepatocytes is due to increased overall levels rather than a redistribution of the protein. Consistent with the in vivo observations, tight junctions were normally formed between primary hepatocytes from all animals (Fig. 2*B*), suggesting that YAP does not influence tight junction formation.

While E-cadherin junctions were absent when two WT or *Yap*-Tg hepatocytes came in contact forming pairs of cells (Fig. 2*C*, WT and Tg, E-cad), the E-cadherin junctions readily formed a continuous band between pairs of *Yap*-KO hepatocyte (Fig. 2*C*, KO, E-cad). The E-cadherin organization between the pairs of *Yap*-KO resembled mature cadherin junctions found in groups of hepatocytes organized into epithelial sheets (60, 64). In small groups of hepatocytes, E-cadherin foci were observed between WT hepatocytes (Fig. 2*D*, WT, E-cad), which resemble E-cadherin organization associated with early stages of junction assembly (64). Still, continuous E-cadherin belts representing mature E-cadherin junctions were present between *Yap*-KO hepatocytes in small groups (Fig. 2*D*, KO, E-cad). In contrast, very few E-cadherin junctions were observed in groups of *Yap*-Tg hepatocytes (Fig. 2*D*, Tg, E-cad). These data indicated that YAP antagonizes E-cadherin junction assembly in cultured primary hepatocytes.

Because a major factor in determining E-cadherin junction assembly is actin cytoskeletal remodeling (11), we explored the junction-associated F-actin organization by costaining E-cadherin and actin filaments. In pairs of WT and *Yap*-Tg-hepatocytes, we observed that circumferential actin rings from each cell ran parallel to the plane of cell-cell contact (Fig. 2*C*, WT and Tg, phalloidin). In *Yap*-KO doublets, actin belts colocalized with linear E-cadherin bands at cell-cell contact regions, which is the common actin architecture of mature E-cadherin junction sites (Fig. 2*C*, KO, phalloidin) (42, 64). In small groups of WT cells, radial actin cables ran perpendicular to the plane of cell-cell contact and connected circumferential actin rings and E-cadherin structures (Fig. 2*D*, WT, phalloidin). This architecture resembles the intermediate "adhesion zipper" structure observed in keratinocytes in the early stages of E-cadherin junction assembly (60). Grouped *Yap*-KO and *Yap*-Tg hepatocytes showed similar actin cytoskeletal organization to that which we observed in their doublet counterparts (Fig. 2*D*, KO and Tg, phalloidin). Therefore, the E-cadherin junction status observed among WT, *Yap*-KO, and *Yap*-Tg hepatocytes is accompanied by specific F-actin organization.

YAP regulates actin cytoskeleton organization. E-cadherin junction status and actin cytoskeletal organization are interdependent so that alterations of one impact the other (11, 63). If YAP affects F-actin organization through E-cadherin junctions, then the actin cytoskeletal architecture in solitary cells should be independent of YAP activity. Alternatively, if YAP modulates the actin network upstream of E-cadherin junctions, then the F-actin organization would be distinct among solitary WT, *Yap*-KO, and *Yap*-Tg hepatocytes. Examination of soli-

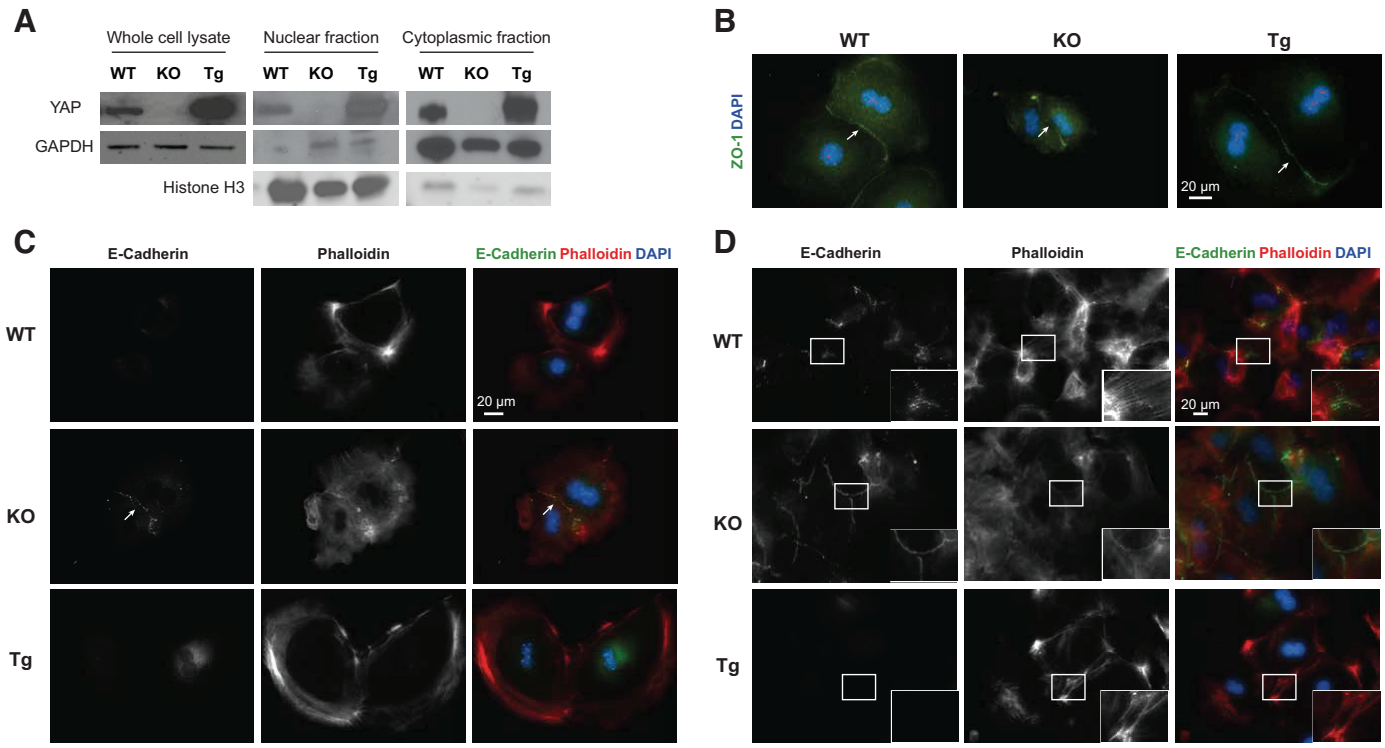

Fig. 2. YAP expression antagonizes E-cadherin junction assembly in primary hepatocytes. *A*: Western analysis reveals YAP levels in whole cell lysates, nuclear fractions and cytoplasmic fractions of *day 1* hepatocytes from WT, *Yap*-KO, and *Yap*-Tg livers. GAPDH serves as loading control and cytoplasmic fraction marker. Histone H3 serves as nuclear fraction marker and loading control. *B*: ZO-1 staining of cultured primary hepatocytes from WT, *Yap*-KO, and *Yap*-Tg mice. *C* and *D*: E-cadherin and F-actin (phalloidin) costaining of cultured primary hepatocytes from WT, *Yap*-KO, and *Yap*-Tg mice in pairs (*C*) or in small groups (*D*). *Insets*: higher magnification of cell-cell contact areas. Note that E-cadherin junction status is accompanied by different actin cytoskeleton organization. WT and *Yap*-Tg hepatocyte doublets do not form E-cadherin junctions with circumferential actin rings run parallel to the plane of cell contacts. *Yap*-KO hepatocyte pairs form E-cadherin junctions with the actin belt colocalizing with the E-cadherin belt (arrows). In WT hepatocyte groups, the intermediate E-cadherin junction structures are observed with radial actin fibers connecting cadherin puncta at one end and circumferential actin rings at the other end. The E-cadherin structure and accompanied actin cytoskeleton structure in grouped *Yap*-Tg and *Yap*-KO hepatocytes are similar to those in doublets.

tary WT, *Yap*-KO, and *Yap*-Tg hepatocytes revealed three distinct types of F-actin organization. The first cytoskeletal organization class (WT-like: actin ring + radial fibers) was mainly found in WT hepatocytes, which had radial actin cables oriented perpendicularly to plasma membrane (arrowheads) and circumferential actin rings that ran parallel to plasma membrane (arrows) (Fig. 3*A*, *top*, WT). The second class (KO-like: radial fibers only) was primarily observed in single *Yap*-KO hepatocytes where only radial actin cables were present (Fig. 3*A*, *top*, KO). The third class (Tg-like: actin ring + short radial fibers) was found in single *Yap*-Tg hepatocytes with highly organized circumferential actin rings and fewer, shorter radial actin cables (Fig. 3*A*, *top*, Tg). Upon closer examination of the circumferential actin rings, we observed multiple actin fibers in the rings (Fig. 3*A*, *bottom*). Compared with the actin rings in WT hepatocytes, the actin bundles in the *Yap*-Tg rings were oriented in a highly parallel fashion (Fig. 3*A*, *bottom*, WT and Tg). Thus, YAP is necessary for circumferential actin ring formation. Too much YAP compromises the radial actin cables. The distribution of each actin organization type among solitary WT, *Yap*-KO, and *Yap*-Tg hepatocytes was quantified in Fig. 3*B*. These data suggest that YAP regulates actin cytoskeleton organization, which in turn affects E-cadherin junction assembly.

YAP promotes myosin II-induced cellular contractility by regulating actin cytoskeleton organization. The circumferential actin bundles in nonmuscle cells are typically contractile due to the presence of myosin II (60). Staining of WT hepatocytes for nonmuscle myosin II heavy chain Myh9 and F-actin revealed that myosin II located on the circumferential actin bundles (Fig. 4*A*). Based on the different circumferential actin bundle structures of WT, *Yap*-KO, and *Yap*-Tg hepatocytes (Fig. 3*A*), we hypothesized that they will have different levels of myosin II activity with *Yap*-Tg>WT>*Yap*-KO. To test this, we measured the cortical elasticity and cortical tension, which provide a quantitative assessment of the myosin II activity in the cells (39).

We measured the cortical elasticity of the fresh isolated hepatocytes using micropipette aspiration (Fig. 4, *B* and *C*). We found that WT hepatocytes had an elastic modulus (E) of 0.19 nN/μm^2. The *Yap*-Tg hepatocytes (E = 0.28 nN/μm^2) were 50% stiffer than WT, while the *Yap*-KO cells (E = 0.099 nN/μm^2) were half as stiff as WT cells. Thus modulating YAP levels generated a threefold dynamic range of cellular elasticity across the three types of hepatocytes. The high cortical elasticity of *Yap*-Tg hepatocytes is consistent with their actin cytoskeleton having high levels of myosin II-induced contractility. In contrast, the low cortical elasticity of *Yap*-KO hepatocytes is consistent with low levels of myosin II-induced contractility.

To confirm the cell autonomous function of YAP in modulating cell mechanics, we modified YAP levels through knockdown and overexpression in AML-12 cells, a hepatocellular cell line. We found that cortical tension, a cell mechanical

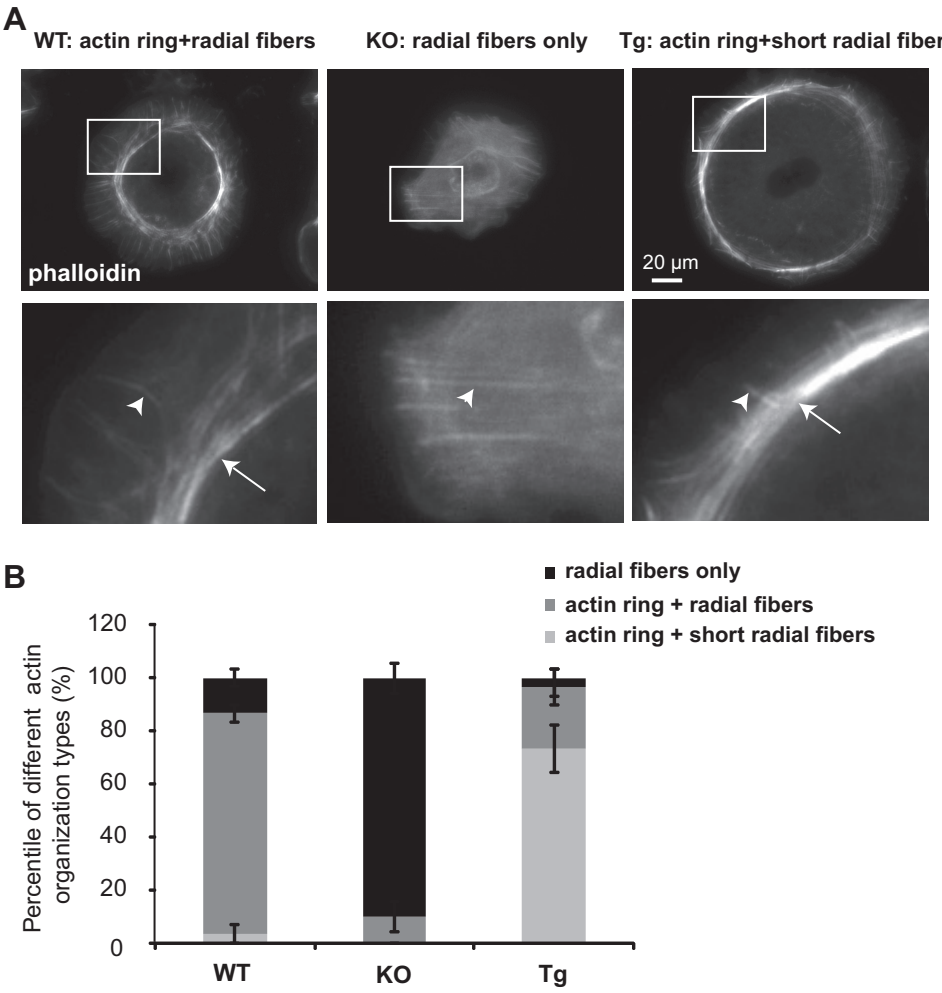

Fig. 3. YAP regulates actin cytoskeleton organization. *A*: representative F-actin organization in solitary WT, *Yap*-KO, and *Yap*-Tg hepatocytes. Higher magnification images of the boxed areas are shown at *bottom*. WT hepatocytes contained radial actin cables (arrow heads) and circumferential actin rings (arrows). The *Yap*-KO hepatocytes possessed radial actin cables only, and the *Yap*-Tg hepatocytes had shorter, less radial actin cables and highly ordered, circumferential actin rings. *B*: quantification of the distributions of 3 F-actin organizations (radial fibers only; actin ring + radial fibers; actin ring + short radial fibers) among 20–30 randomly selected solitary WT, *Yap*-K, and *Yap*-Tg hepatocytes. Bars represent mean ± SE (n = 3 mice from each genotype).

parameter related to cortical elasticity, was altered in a manner similar to the changes in cortical elasticity observed in primary hepatocytes (Fig. 4*D*).

The cell shape dynamics of the primary hepatocytes were assessed with 48-h time-lapse microscopy and quantification of membrane defragmentation events. In WT hepatocytes, lamellipodial protrusions were continuously formed and then either retracted or the cell body followed, resulting in cell motility (Fig. 4*E*, WT; Supplemental Video S1; Supplemental Material for this article is available online at the Journal website). In *Yap*-KO cells, the lamellipodial protrusions extended until a neck region formed, often pinching off fragments of cytoplasm (similar to a Laplace pressure-mediated neck-thinning instability; Ref. 52) (Fig. 4*E*, KO; Supplemental Video S2). In *Yap*-Tg cells, the cell cortex was particularly stable as lamellipodial protrusion and fragmentation events were rare (Fig. 4*E*, Tg; Supplemental Video S3). The lamellae fragmentation events were quantified per 100 cells for each cell type (Fig. 4*F*). These data indicated *Yap*-KO hepatocytes have extreme cortical instability, which is likely due to the low level of myosin II activity. Moreover, the first step in E-cadherin junction assembly is an opportunistic event resulting from the exploratory behavior of cells extending lamellipodia and membrane ruffles (10). The stabilized cell cortex of *Yap*-Tg hepatocytes is expected to reduce the formation of cell-cell contacts.

Physical modeling predicts that YAP antagonizes cell-cell adhesion by regulating actomyosin contractility. Based on the cortical elasticity data (Fig. 4, *B* and *C*), we employed analytical modeling to predict the cell morphological changes that are dependent on YAP levels (Fig. 5). This model predicts that higher cortical tension and elasticity (*Yap*-Tg-like) favor round, nonadherent cell morphology, whereas lower cortical tension and elasticity (*Yap*-KO-like) favor cells to form straighter surfaces and favor cell-cell adhesion. Hence, the combination of cortical tension and adhesion energy predicts a decrease of cell-cell adhesion in *Yap*-Tg hepatocytes and an increase of cell-cell adhesion in *Yap*-KO hepatocytes, which is in agreement with the observations of reduced and increased E-cadherin junction assembly in *Yap*-Tg and *Yap*-KO hepatocytes, respectively.

YAP antagonizes cell-cell adhesion. To explore whether the physical model correctly predicts altered ability to form cell-cell adhesions in each of the cell types, we employed the hanging drop assay to functionally determine whether YAP antagonizes cell-cell adhesion. The hanging drop assay measures the cell aggregation ability and has been previously used to characterize the role of E/N cadherin, Rac1, and Merlin in regulating cell-cell adhesion (21, 37, 45). We used freshly isolated primary hepatocytes from WT, *Yap*-KO, and *Yap*-Tg (after 3 days of Dox feeding) animals to perform the assay. At

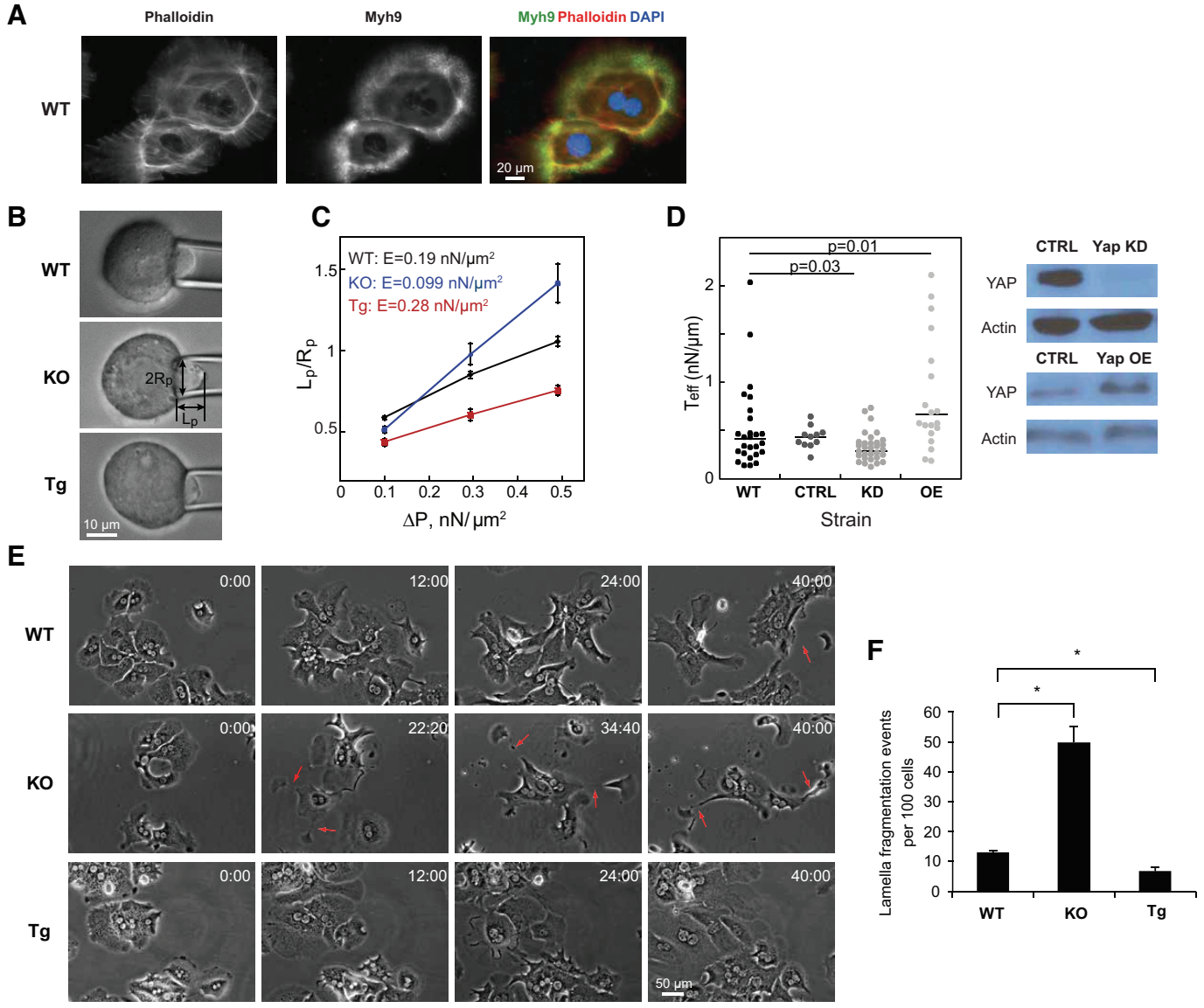

Fig. 4. YAP promotes myosin II-induced cellular contractility. *A*: WT hepatocytes examined by immunofluorescence staining of F-actin (phalloidin) and MYH9. Note that MYH9 colocalizes with circumferential actin rings. *B*: representative images of micropipette aspiration measurements (MPA) of WT, *Yap*-KO, and *Yap*-Tg hepatocytes. Hepatocytes were aspirated at pressure $\Delta P = 0.5$ nN/μm^2. The length (L_p) and the width ($2R_p$) of the aspirated portion were measured with ImageJ software. *Yap*-KO hepatocytes yielded larger L_p values while *Yap*-Tg hepatocytes yielded smaller L_p values when aspirated into the same pipette at the same pressure compared with a WT hepatocyte. *C*: determination of the Young's modulus of elasticity (E) from MPA measurements. *Yap*-KO hepatocytes have the lowest Young's modulus (most deformable), *Yap*-Tg hepatocytes have the highest Young's modulus (least deformable), and WT hepatocytes are intermediate; 10–30 hepatocytes from each genotype were included in the measurements. *D*: cortical tension of AML12 cells without lentiviral transfection (WT), with lentiviral transfection of plasmids encoding control (eGFP) plasmid (CTRL), *Yap* shRNA (KD), and *Yap* cDNA (OE). Western analysis of YAP confirmed the knockdown and overexpression of YAP protein in AML12 cells. Note AML12 cells with YAP knockdown showed lower cortical tension while with YAP overexpression showed higher cortical tension, compared with control cells; 10–30 cells from each treatment were included in the measurements. *P* values were calculated using the two-way ANOVA and a Fisher's least significant difference posttest. *E*: morphology changes of WT, *Yap*-KO, and *Yap*-Tg hepatocytes were imaged by time-lapse phase-contrast microscopy over a 48-h period, starting from *day 0*. Representative images from the indicated time points are shown. The *Yap*-KO hepatocytes displayed long lamellipodial protrusions, which fragmented as the lamellipodia extended from the cell body (breaking points indicated by red arrows). The *Yap*-Tg hepatocytes maintained shorter, broader lamella compared with WT hepatocytes. *E*: quantification of lamella fragmentation events in WT, *Yap*-KO, and *Yap*-Tg hepatocytes. Bars represent mean ± SE ($n = 3$ mice from each genotype). *$P < 0.05$, compared with WT by one-way ANOVA and Fisher's least significant difference posttest. Also see Supplemental Videos S1–S3.

the beginning of the experiment, hepatocytes from all the animals were present as single cells (20%), small clusters (2–5 cells, 60%), and large clusters (>5 cells, 20%) (Fig. 6, *A* and *B*, 0 h). The fraction of WT hepatocytes in large clusters (>5 cells) increased to 48% at 3 h (Fig. 6, *A* and *B*, 3 h). Hepatocytes from *Yap*-KO animals formed large clusters of more than five cells more quickly, with 82% of cells in large clusters, while hepatocytes from *Yap*-Tg animals formed large clusters more slowly with 33% of cells in large clusters at 3 h (Fig. 6, *A* and *B*, 3 h). Thus YAP antagonizes cell-cell adhesion as predicted by the model (Fig. 5) and these findings are consistent with E-cadherin junction formation results (Fig. 2).

YAP regulates actin cytoskeleton organization and E-cadherin junction formation by promoting myosin light chain expression. To understand how YAP regulates actomyosin cytoskeleton organization, we analyzed the published microarray data and literature (9, 59, 67) on YAP regulated gene expression and focused on 10 genes (*Anln*, *Diaph3*, *Ect2*, *Formin1*, *FLNA*, *Myl9*, *Myh9*, *Myh10*, *RacGAP1*, and *Kif23*) that are involved in actomyosin cytoskeleton regulation. We

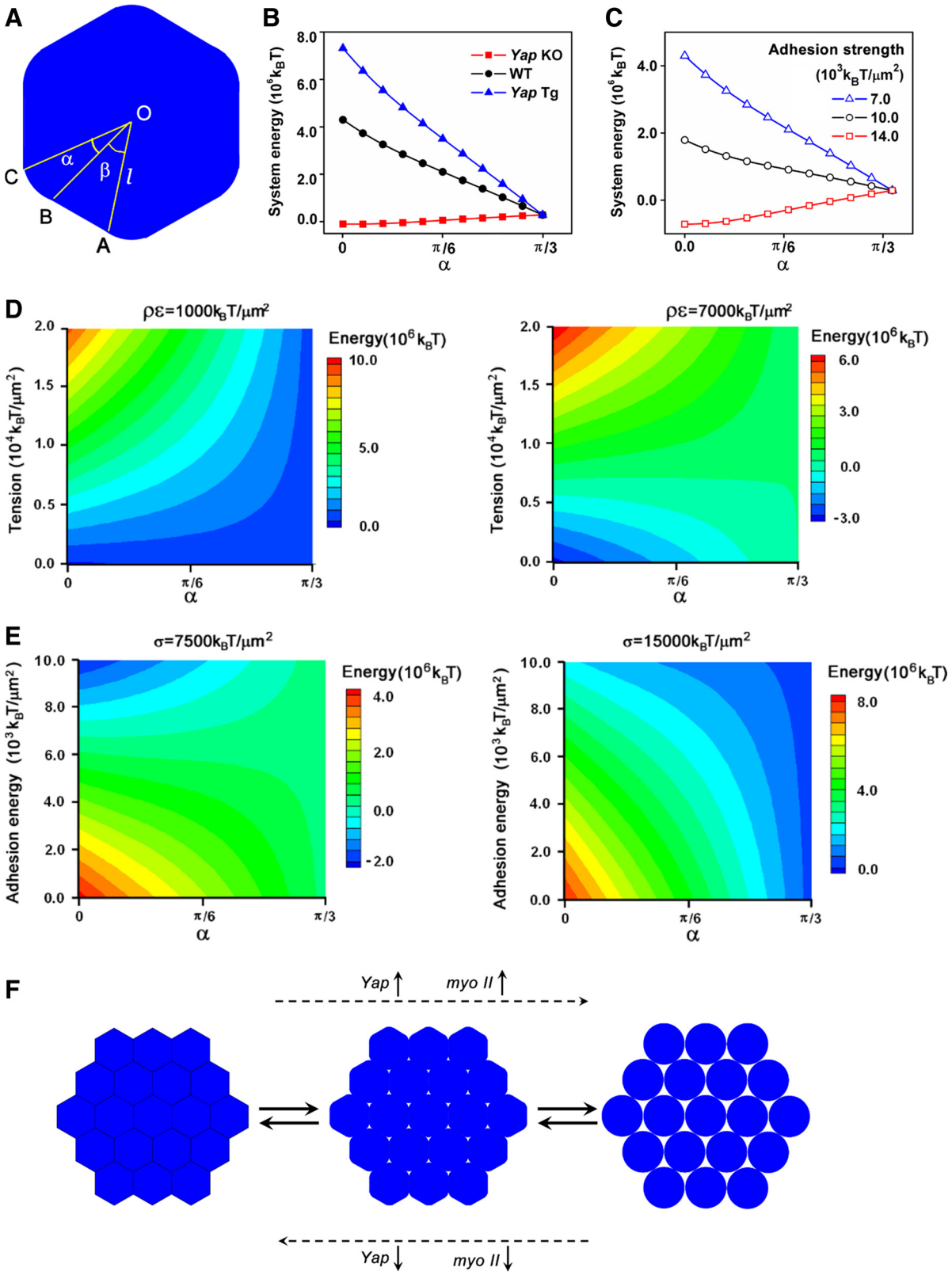

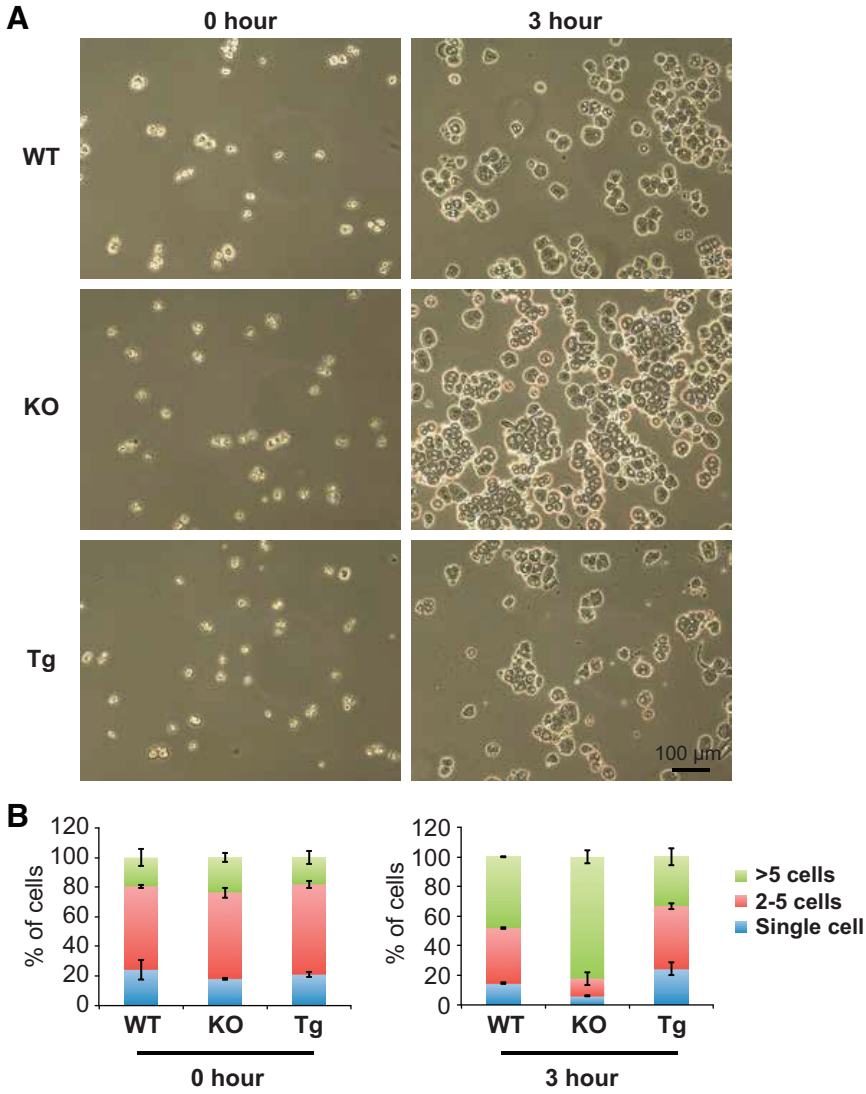

Fig. 6. YAP antagonizes cell-cell adhesion. A hanging drop assay, which provides a functional readout on cell-cell adhesion, was performed with freshly isolated hepatocytes from WT, *Yap*-KO, and *Yap*-Tg (Dox feeding for 3 days) animals. *A*: representative fields at 0 and 3 h are shown. *B*: graph show the percentage of cells in single cells, aggregates of 2–5 cells and clusters of >25 cells at the time points indicated. For each time point, 300–500 cells were scored. Bars represent mean ± SE (n = 3 mice from each genotype).

measured the expression of these genes in WT, *Yap*-Tg, and *Yap*-KO *day 1* hepatocytes, with known YAP targets *CTGF* and *Cyr61* (46) as positive controls (Fig. 7*A*). The expression of *Myl9* showed the same trend as that of *CTGF* and *Cyr61*. The expression of *Diaph3* was significantly suppressed in *Yap*-KO hepatocytes, consistent with observations in cancer-associated fibroblasts (9). YAP overexpression significantly induced the expression of *RacGAP1* and *Kif23*. We confirmed MYL9 protein and phosphorylation (P-Ser19) levels were dependent on YAP in primary hepatocytes (Fig. 7*B*). Significantly, YAP regulated Myl9 expression in a TEAD-dependent manner (Fig. 7*C*), which further confirmed that Myl9 is a downstream effector of YAP. To determine whether increased MYL9 activity was responsible for YAP-regulated actomyosin cytoskeleton organization in primary hepatocytes, we reduced MYL9 activity by treating *Yap*-Tg hepatocytes with the myosin light chain kinase (MLCK) inhibitor ML-7 (5 μM) or the ROCK inhibitor Y27632 (25 μM) (7,

Fig. 5. A physical model of YAP's indirect regulation of cell adhesion and morphology. *A*: representative cell shape used for physical modeling has 6-fold symmetry ($\alpha + \beta = \pi/3$). $\alpha = 0$ and $\alpha = \pi/3$ correspond to the configurations shown in *F*, *left* and *right*, respectively. *B*: system energy determined by *Eq. 1* for WT, *Yap*-KO, and *Yap*-Tg cells where the tensions are converted from the measured Young's modulus shown in Fig. 4*C*, and the cell-cell adhesion strength is 7,000 $k_BT/\mu m^2$ for all cases. *C*: system energy for cells having WT tension, but with different cell-cell adhesion strengths as indicated in the graph. *D*: contour map of the energy calculated for systems with different cell-cell adhesion strengths. The energy contours are calculated for adhesion strengths of 1,000 and 7,000 $k_BT/\mu m^2$, respectively, using *Eq. 1*. $\alpha = 0$ and $\alpha = \pi/3$ correspond to the configurations of hexagonal and circular cross-section, respectively. The system always favors the configuration with the lowest energy. *E*: contour map of the energy calculated for systems with different cortical tensions. The cortical tension values used for calculating the energy contour were 7,500 and 15,000 $k_BT/\mu m^2$, respectively, using *Eq. 1*. As in *D*, $\alpha = 0$ and $\alpha = \pi/3$ correspond to the configurations of hexagonal and circular cross-section, respectively, and the system always favors the configuration with the lowest energy. *F*: cartoon depicts the results of the computational model of YAP-regulated cell mechanics on epithelial adhesion. Cells with increased elasticity and cortical tension due to elevated myosin II activity have lower cell-cell adhesion and are more circular in shape. The *Yap* knockout leads to decreased myosin II activity, which favors the formation cell-cell adhesion and hexagonal cells.

55). After a 24-h treatment to *day 0 Yap*-Tg hepatocytes, we found that inhibition of MLCK or ROCK restored E-cadherin junction assembly in *Yap*-Tg hepatocyte doublets. From phalloidin staining, ML-7 and Y27632 treatment disrupted the circumferential actin bundles but left other types of stress fibers intact (Fig. 7*D*). These data indicate that YAP regulates actomyosin cytoskeleton organization by promoting MYL9 expression.

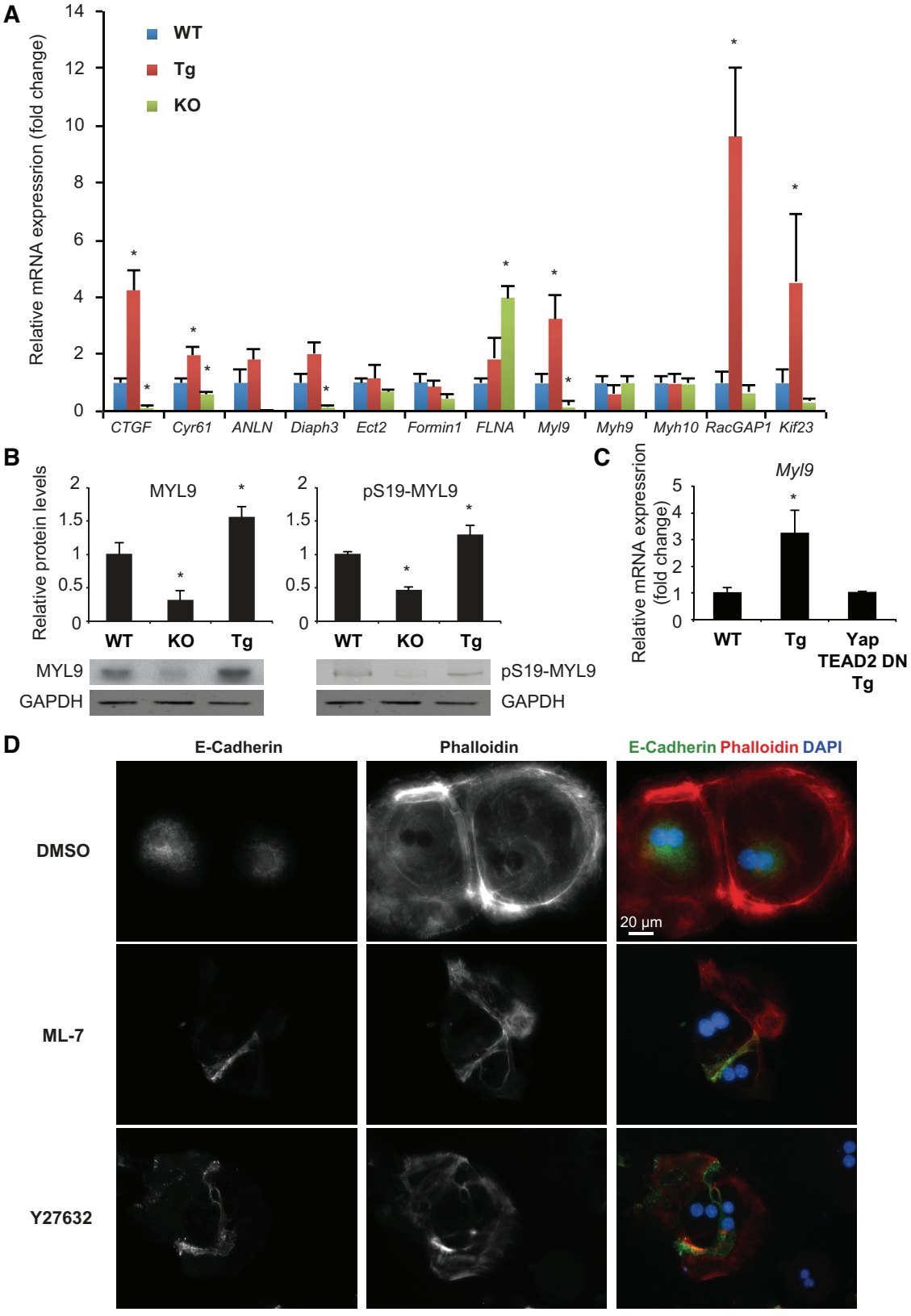

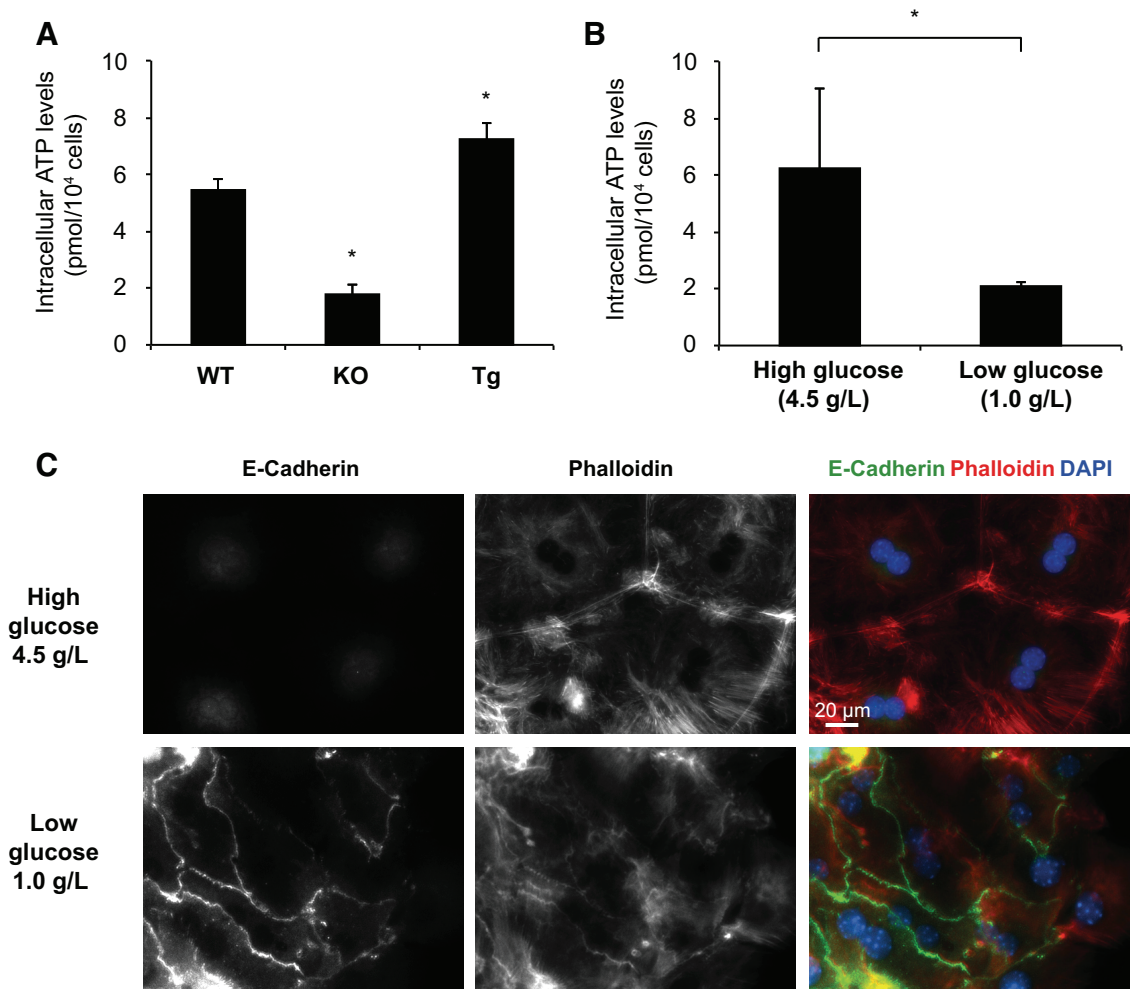

Fig. 8. YAP regulates actin cytoskeleton organization and E-cadherin junction formation by increasing intracellular ATP concentration. *A*: graph shows the intracellular ATP levels of 1×10^4 freshly isolated hepatocytes from WT, *Yap*-KO, and *Yap*-Tg livers. Bars represent mean ± SE ($n = 3$ mice from each genotype). *$P < 0.05$, compared with WT by one-way ANOVA and Fisher's least significant difference posttest. *B*: graph shows the intracellular ATP levels of *day 1* hepatocytes with high glucose medium (4.5 g/l) or low glucose medium (1 g/l) from *Yap*-Tg livers. Bars represent mean ± SE ($n = 3$ mice from each genotype). *$P < 0.05$ by unpaired *t*-test. *C*: E-cadherin and F-actin (phalloidin) staining of *day 1* hepatocytes high glucose medium (4.5 g/l) or low glucose medium (1 g/l) from *Yap*-Tg livers. Note the E-cadherin formation and absence of circumferential actin rings in *Yap*-Tg hepatocytes cultured with low glucose medium.

YAP regulates actin cytoskeleton organization and E-cadherin junction formation by increasing intracellular ATP concentration. Myosin is a motor protein that uses the energy from ATP hydrolysis to pull on actin filaments. Therefore, the availability of ATP is crucial for myosin activity. Recently, YAP was found to increase glycolysis by increasing the expression of the glucose transporter GLUT3 (62), which could have an impact on the energy state of the cell. Therefore, we measured the ATP levels in the *Yap*-KO and *Yap*-Tg cells compared with WT cells to determine if they correlate with the altered cell morphology, including adherens junction formation. We found that indeed the intracellular ATP levels of newly isolated hepatocytes from WT, *Yap*-KO, and *Yap*-Tg (Dox 3 days) mice had altered ATP levels that correlated with Yap expression (Fig. 8*A*). To determine whether the altered ATP levels contributed to the altered cytoskeleton and junction formation in *Yap*-Tg hepa-

Fig. 7. YAP promotes myosin light chain expression. *A*: graph shows the expression of genes of interest in *day 1* hepatocytes from WT, *Yap*-KO, and *Yap*-Tg livers. Bars represent mean ± SE ($n = 3$ mice from each genotype). *$P < 0.05$, compared with WT by one-way ANOVA and unpaired *t*-test. *B*: Western analysis shows levels of MYL9 and pS19-MYL9 in *day 1* hepatocytes from WT, *Yap*-KO, and *Yap*-Tg livers. Graphs show the quantification of MYL9, pS19-MYL9 protein levels. Bars represent mean ± SE ($n = 3$ mice from each genotype). *$P < 0.05$, compared with WT by one-way ANOVA and Fisher's least significant difference posttest. *C*: graph shows the expression levels of *Myl9* in *day 1* hepatocytes from WT, *Yap*-Tg, and *Yap/TEAD2 DN*-Tg mice. Note that YAP-induced *Myl9* expression was inhibited by coexpressing a dominant negative form of TEAD2. Bars represent mean ± SE ($n = 3$ mice from each genotype). *$P < 0.05$, compared with WT using a one-way ANOVA and Fisher's least significant difference posttest. *D*: E-cadherin and phalloidin staining of *day 1 Yap*-Tg hepatocytes treated with DMSO (vehicle control), 5-μM myosin light-chain kinases inhibitor ML-7 and 25-μM Rho-associated protein kinase (ROCK) inhibitor Y27632 for 24 h. ML-7- and Y27632-treated *Yap*-Tg doublet hepatocytes show similar F-actin organization and E-cadherin junction formation as *Yap*-KO doublet hepatocytes.

tocytes, we cultured *Yap*-Tg hepatocytes in low glucose medium (1 g/l glucose) (31). Culturing in low glucose medium for 24 h reduced intracellular ATP levels of *Yap*-Tg hepatocytes compared with those cultured in high glucose medium (4.5 g/l) (Fig. 8*B*). The low glucose medium also disrupted circumferential actin bundles formation and restored E-cadherin junction formation in *Yap*-Tg hepatocytes (Fig. 8*C*).

DISCUSSION

In this study, we demonstrated that by promoting *Myl9* expression and cellular ATP production, YAP upregulates nonmuscle myosin II activity and promotes cytoarchitectural integrity in hepatocytes. Increased myosin II activity leads to greater contractile stress fiber (circumferential actin bundles) formation, increased cell stiffness, and a more stabilized cell cortex (reflected by reduced lamella fragmentation events). This cellular architecture in turn antagonizes cell-cell adhesion as predicted by the physical model and as demonstrated in the hanging drop assay and E-cadherin junction assembly in vitro. Reducing cell-cell adhesion between hepatocytes is expected to induce increased bile-blood barrier permeability (28). In vivo, we observed YAP overexpression in hepatocytes caused jaundice, which was likely due to increased bile-blood barrier permeability, while in *Yap*-KO mice, the bile-blood barrier permeability was reduced after bile-duct ligation. Thus, YAP antagonizes cell-cell adhesion in vitro correlates with the phenotypes we observed in vivo in *Yap*-KO and *Yap*-Tg mice.

YAP regulates the organization of actin cytoskeleton. We found that two kinds of stress fiber (radial fibers and circumferential actin bundles, also called dorsal fibers and transverse arcs; Ref. 58) are present in WT primary hepatocytes. By comparing WT with *Yap*-Tg and *Yap*-KO hepatocytes, we found that YAP promoted circumferential actin bundle/transverse arc formation and antagonized radial fiber/dorsal fiber formation. Each of the stress fiber types has distinct functions due to their unique structures (58). The dorsal fibers usually do not contain myosin II, so they are expected to be less contractile. The main function of the dorsal fibers is to provide the link between focal adhesion/cell-cell junctions to the transverse arcs. Transverse arcs are contractile actomyosin bundles that transmit contractile force to the surrounding environment through their connections with dorsal stress fibers. Transverse arcs provide the linkage between lamellipodia and the cell body and are required for coordinated cell migration. YAP has been shown to increase cellular contractility though the structural details have not previously been elucidated (9). Our study provides some of the structural mechanisms by which YAP increases cellular elasticity and contractility by promoting contractile transverse arcs formation. The loss of these structures and the associated reduction of cortical elasticity and tension are likely to account for the high lamellipodia fragmentation events observed in the *Yap*-KO hepatocytes.

By regulating actin cytoskeleton organization, YAP indirectly affects E-cadherin junction assembly. Studies of the cell-cell junction formation with cultured cells suggested the following steps of actin organization during cell-cell junction formation (10): *1*) before cell-cell contact, epithelial cells extend membrane protrusions driven by actin polymerization to explore the environment and generate initial contacts; *2*) cadherin puncta form at the tips of initial contacts and are connected to the circumferential actin rings via radial actin fibers; and *3*) as cell-cell contacts mature, actin remodels along the contact resulting in formation of the adhesion belt. Due to different levels of cellular contractility, *Yap*-KO hepatocytes showed extremely high frequency of membrane protrusions, which significantly increase the opportunity for forming cell-cell contacts. In contrast, *Yap*-Tg hepatocytes showed a low frequency of membrane protrusions, reducing their opportunity to initiate E-cadherin junctions. Second, radial actin fibers directly contact E-cadherin, suggesting the important role of radial fibers during junction formation. Compromised radial fiber formation in solitary cells and the absence of radial fibers at the cell-cell contacts sites of *Yap*-Tg hepatocytes may cause the defects of E-cadherin junction assembly.

Consistent with our observations, deletion of YAP's negative regulator, *Nf2*, which leads to an increase YAP activity, destabilized adherens junction in vivo and in vitro (25, 43, 45). Although it was suggested that NF2 (a.k.a. Merlin) stabilized adherens junctions through interactions with α-catenin and actin cytoskeleton (25, 43), neuroepithelial cells that lose NF2 early in gestation fail to assemble adherens junctions and are prone to detachment from the apical surface, while neuroepithelial cells that lose NF2 late in gestation maintain adherens junctions (45). These findings suggest that NF2 is required for the assembly, but not the maintenance, of adherens junctions, which contrasts with the phenotype of mouse embryos whose junctional complex core components are deleted (6). Thus, while NF2 is unlikely to serve as a core structural component of adherens junctions, it might permit adherens junction assembly, at least partially through its inhibition of YAP.

External mechanical cues have been shown to impact YAP activity. For example, high extracellular matrix (ECM) stiffness or large adhesion foci induce YAP activation, which is indicated by increased nuclear accumulation. In contrast, low ECM stiffness or small adhesion foci lead to YAP inactivation, as demonstrated by cytoplasmic retention (8, 19). Disturbing

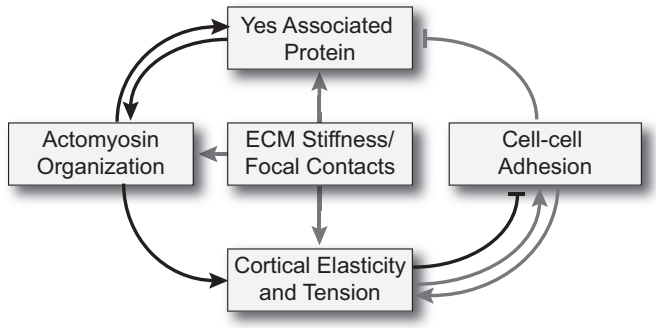

Fig. 9. YAP-based feedback system for cell mechanics modulation. YAP is positioned in a biomechanical feedback system where YAP modulates actomyosin architecture, which specifies cortical elasticity and tension and regulates cell-cell adhesion. Cortical tension and elasticity has a complex, biphasic relationship with cell-cell adhesion. Low levels of cortical tension promote cell-cell adhesion, and this tension increases as adhesions are formed (the arrows indicate this positive feedback) (27, 63). However, if the cortical tension is too high, then the tension is a barrier to forming adhesions. The inhibitory bar reflects this case, which we observed in the Yap overexpression scenario hepatocytes. Imposed mechanical stresses or alterations in the cell architecture can in turn modulate YAP activity. Black activating (arrows) and inhibitory lines represent YAP's connections defined in this study, and the gray lines represent YAP's previously defined connections. ECM, extracellular matrix.

the cell adhesion mechanical receptors, such as the E-cadherin/α-catenin complexes, decreases YAP phosphorylation and stimulates YAP nuclear accumulation (38). Conversely, formation of E-cadherin junctions triggers LATS activation and YAP phosphorylation (2), and changes to actin cytoskeletal dynamics impact YAP activity (22, 53). These studies demonstrate that YAP functions downstream of changes in cytoarchitecture that may be induced by external mechanical stimuli. Our study demonstrates that YAP itself is a rheostat for cytoarchitecture, manifested in altered cell elasticity and tension due to the redistribution of myosin II, which in turn modulates cell adhesivity. These two roles for YAP are not mutually exclusive but instead point toward a system in which YAP functions in a positive feedback that integrates cytoarchitecture and cell mechanics with adhesion and cellular mechanosensing ability (Fig. 9). As a consequence of this feedback system, YAP is exquisitely poised to control a hepatocyte's ability to tune its mechanical properties in response to a changing environment, which include alterations in the ECM stiffness and forced sharing by neighboring cells.

Our study identified an intriguing implication of YAP on cell mechanics and behavior. Cellular ATP levels varied with YAP levels and the myosin light chain (Myl9) expression decreased with loss of YAP. ATP levels in cells typically range from 1 to 10 mM. At 1 mM ATP and above, the ATP-binding rate on myosin II saturates so that further increases in ATP concentrations should have a nominal impact on myosin II activity (40). If the reduction in ATP levels observed in the Yap-KO cells managed to reduce ATP levels below the saturation level, then the motors would remain bound for a longer period of time, increasing the myosin motor's duty ratio and increasing the fraction of heads in the load-bearing state. In this scenario, the anticipated consequence is that the system would become more contractile with increased cortical tension and elasticity. However, the opposite is observed probably due in part to the loss of myosin II light chain (Myl9), which would lead to inactive motors. More likely, the altered energy state of the cell observed by modulating Yap activity leads to differential signaling within the cell that leads to altered contractility.

Overall, in addition to its role in promoting cell proliferation and survival, YAP regulates actin cytoskeleton organization and, in turn, tunes E-cadherin-junction assembly. The actin cytoskeleton is a major coordinator of many types of cell behaviors including morphology, division, motility, and cell adhesion.

ACKNOWLEDGMENTS

D. Pan is an investigator of the Howard Hughes Medical Institute.

For correspondence regarding cortical elasticity, cortical tension measurements, and physical model simulation: D. Robinson (dnr@jhmi.edu). For correspondence regarding hepatocyte isolation, culture, and other in vitro analysis: R. Anders (rander54@jhmi.edu).

GRANTS

This study was supported by National Institutes of Health Grants DK-080736 and DK-081417 (to R. A. Anders) and GM-66817 (to D. N. Robinson). This study was also supported by startup funding to H. Bai through Dr. Nicholas C. Hightower Centennial Chair of Gastroenterology from Baylor Scott & White Health and a Veterans Affairs Research Career Scientist Award, and Veterans Affairs Merit Award (5I01BX000574; to G. Alpini). This material is the result of work supported by resources at the Central Texas Veterans Health Care System. The views expressed in this article are those of the authors and do not necessarily represent the views of the Department of Veterans Affairs.

DISCLOSURES

No conflicts of interest, financial or otherwise, are declared by the author(s).

AUTHOR CONTRIBUTIONS

H.B., T.L., D.N.R., and R.A.A. conception and design of research; H.B., Q.Z., A.S., T.L., Y.R., B.G., Y.L., N.E.J., and N.Z. performed experiments; H.B., Q.Z., A.S., T.L., Y.R., B.G., Y.L., N.E.J., and N.Z. analyzed data; H.B., Q.Z., A.S., T.L., Y.R., B.G., N.W., D.P., G.A., D.N.R., and R.A.A. interpreted results of experiments; H.B., Q.Z., A.S., T.L., N.W., and D.N.R. prepared figures; H.B. drafted manuscript; H.B., Q.Z., A.S., T.L., Y.R., B.G., Y.L., T.-L.W., N.Z., D.P., G.A., D.N.R., and R.A.A. edited and revised manuscript; H.B., Q.Z., A.S., T.L., Y.R., B.G., Y.L., T.-L.W., N.Z., D.P., G.A., D.N.R., and R.A.A. approved final version of manuscript.

REFERENCES

1. **Angermann BR, Klauschen F, Garcia AD, Prustel T, Zhang F, Germain RN, Meier-Schellersheim M.** Computational modeling of cellular signaling processes embedded into dynamic spatial contexts. *Nat Meth* 9: 283–289, 2012.
2. **Aragona M, Panciera T, Manfrin A, Giulitti S, Michielin F, Elvassore N, Dupont S, Piccolo S.** A mechanical checkpoint controls multicellular growth through YAP/TAZ regulation by actin-processing factors. *Cell* 154: 1047–1059, 2013.
3. **Azzolin L, Panciera T, Soligo S, Enzo E, Bicciato S, Dupont S, Bresolin S, Frasson C, Basso G, Guzzardo V, Fassina A, Cordenonsi M, Piccolo S.** YAP/TAZ incorporation in the beta-catenin destruction complex orchestrates the Wnt response. *Cell* 158: 157–170, 2014.
4. **Bai H, Zhang N, Xu Y, Chen Q, Khan M, Potter JJ, Nayar SK, Cornish T, Alpini G, Bronk S, Pan D, Anders RA.** Yes-associated protein regulates the hepatic response after bile duct ligation. *Hepatology* 56: 1097–1107, 2012.
5. **Bischofs IB, Schmidt SS, Schwarz US.** Effect of adhesion geometry and rigidity on cellular force distributions. *Phys Rev Lett* 103: 048101, 2009.
6. **Boggetti B, Niessen CM.** Adherens junctions in mammalian development, homeostasis and disease: lessons from mice. *Subcell Biochem* 60: 321–355, 2012.
7. **Bresnick AR.** Molecular mechanisms of nonmuscle myosin-II regulation. *Curr Opin Cell Biol* 11: 26–33, 1999.
8. **Calvo F, Ege N, Grande-Garcia A, Hooper S, Jenkins RP, Chaudhry SI, Harrington K, Williamson P, Moeendarbary E, Charras G, Sahai E.** Mechanotransduction and YAP-dependent matrix remodelling is required for the generation and maintenance of cancer-associated fibroblasts. *Nat Cell Biol* 15: 637–646, 2013.
9. **Calvo F, Ege N, Grande-Garcia A, Hooper S, Jenkins RP, Chaudhry SI, Harrington K, Williamson P, Moeendarbary E, Charras G, Sahai E.** Mechanotransduction and YAP-dependent matrix remodelling is required for the generation and maintenance of cancer-associated fibroblasts. *Nat Cell Biol* 15: 637–646, 2013.
10. **Cavey M, Lecuit T.** Molecular bases of cell-cell junctions stability and dynamics. *Cold Spring Harb Perspect Biol* 1: a002998, 2009.
11. **Cavey M, Lecuit T.** Molecular bases of cell-cell junctions stability and dynamics. *Cold Spring Harb Perspect Biol* 1: a002998, 2009.
12. **Dai Z, Zhu WG, Morrison CD, Brena RM, Smiraglia DJ, Raval A, Wu YZ, Rush LJ, Ross P, Molina JR, Otterson GA, Plass C.** A comprehensive search for DNA amplification in lung cancer identifies inhibitors of apoptosis cIAP1 and cIAP2 as candidate oncogenes. *Hum Mol Genet* 12: 791–801, 2003.
13. **Das A, Fischer RS, Pan D, Waterman CM.** YAP nuclear localization in the absence of cell-cell contact is mediated by a filamentous actin-dependent, myosin II- and phospho-Yap-independent pathway during extracellular matrix mechanosensing. *J Biol Chem* 291: 6096–6110, 2016.
14. **Dash A, Simmers MB, Deering TG, Berry DJ, Feaver RE, Hastings NE, Pruett TL, LeCluyse EL, Blackman BR, Wamhoff BR.** Hemodynamic flow improves rat hepatocyte morphology, function, and metabolic activity in vitro. *Am J Physiol Cell Physiol* 304: C1053–C1063, 2013.
15. **de Rooij J, Kerstens A, Danuser G, Schwartz MA, Waterman-Storer CM.** Integrin-dependent actomyosin contraction regulates epithelial cell scattering. *J Cell Biol* 171: 153–164, 2005.
16. **Derganc J, Bozic B, Svetina S, Zeks B.** Stability analysis of micropipette aspiration of neutrophils. *Biophys J* 79: 153–162, 2000.
17. **Discher DE, Boal DH, Boey SK.** Simulations of the erythrocyte cytoskeleton at large deformation. II. Micropipette aspiration. *Biophys J* 75: 1584–1597, 1998.

18. **Dong J, Feldmann G, Huang J, Wu S, Zhang N, Comerford SA, Gayyed MF, Anders RA, Maitra A, Pan D.** Elucidation of a universal size-control mechanism in Drosophila and mammals. *Cell* 130: 1120–1133, 2007.
19. **Dupont S, Morsut L, Aragona M, Enzo E, Giulitti S, Cordenonsi M, Zanconato F, Le Digabel J, Forcato M, Bicciato S, Elvassore N, Piccolo S.** Role of YAP/TAZ in mechanotransduction. *Nature* 474: 179–183, 2011.
20. **Effler JC, Kee YS, Berk JM, Tran MN, Iglesias PA, Robinson DN.** Mitosis-specific mechanosensing and contractile-protein redistribution control cell shape. *Curr Biol* 16: 1962–1967, 2006.
21. **Ehrlich JS, Hansen MD, Nelson WJ.** Spatio-temporal regulation of Rac1 localization and lamellipodia dynamics during epithelial cell-cell adhesion. *Dev Cell* 3: 259–270, 2002.
22. **Fernandez BG, Gaspar P, Bras-Pereira C, Jezowska B, Rebelo SR, Janody F.** Actin-Capping Protein and the Hippo pathway regulate F-actin and tissue growth in Drosophila. *Development* 138: 2337–2346, 2011.
23. **Gao T, Zhou D, Yang C, Singh T, Penzo-Mendez A, Maddipati R, Tzatsos A, Bardeesy N, Avruch J, Stanger BZ.** Hippo signaling regulates differentiation and maintenance in the exocrine pancreas. *Gastroenterology* 144: 1543–1553, 1553 e1541, 2013.
24. **Georgiev P, Navarini AA, Eloranta JJ, Lang KS, Kullak-Ublick GA, Nocito A, Dahm F, Jochum W, Graf R, Clavien PA.** Cholestasis protects the liver from ischaemic injury and post-ischaemic inflammation in the mouse. *Gut* 56: 121–128, 2007.
25. **Gladden AB, Hebert AM, Schneeberger EE, McClatchey AI.** The NF2 tumor suppressor, Merlin, regulates epidermal development through the establishment of a junctional polarity complex. *Dev Cell* 19: 727–739, 2010.
26. **Halder G, Johnson RL.** Hippo signaling: growth control and beyond. *Development* 138: 9–22, 2011.
27. **Harris AR, Peter L, Bellis J, Baum B, Kabla AJ, Charras GT.** Characterizing the mechanics of cultured cell monolayers. *Proc Natl Acad Sci USA* 109: 16449–16454, 2012.
28. **Herr KJ, Tsang YH, Ong JW, Li Q, Yap LL, Yu W, Yin H, Bogorad RL, Dahlman JE, Chan YG, Bay BH, Singaraja R, Anderson DG, Koteliansky V, Viasnoff V, Thiery JP.** Loss of alpha-catenin elicits a cholestatic response and impairs liver regeneration. *Sci Rep* 4: 6835, 2014.
29. **Hilgenfeldt S, Erisken S, Carthew RW.** Physical modeling of cell geometric order in an epithelial tissue. *Proc Natl Acad Sci USA* 105: 907–911, 2008.
30. **Hochmuth RM.** Micropipette aspiration of living cells. *J Biomech* 33: 15–22, 2000.
31. **Honda K, Kato K, Dairaku N, Iijima K, Koike T, Imatani A, Sekine H, Ohara S, Matsui H, Shimosegawa T.** High levels of intracellular ATP prevent nitric oxide-induced apoptosis in rat gastric mucosal cells. *Int J Exp Pathol* 84: 281–288, 2003.
32. **Ivanov AI.** Actin motors that drive formation and disassembly of epithelial apical junctions. *Front Biosci* 13: 6662–6681, 2008.
33. **Ivanov AI, Bachar M, Babbin BA, Adelstein RS, Nusrat A, Parkos CA.** A unique role for nonmuscle myosin heavy chain IIA in regulation of epithelial apical junctions. *PLoS One* 2: e658, 2007.
34. **Ivanov AI, McCall IC, Parkos CA, Nusrat A.** Role for actin filament turnover and a myosin II motor in cytoskeleton-driven disassembly of the epithelial apical junctional complex. *Mol Biol Cell* 15: 2639–2651, 2004.
35. **Katsamba P, Carroll K, Ahlsen G, Bahna F, Vendome J, Posy S, Rajebhosale M, Price S, Jessell TM, Ben-Shaul A, Shapiro L, Honig BH.** Linking molecular affinity and cellular specificity in cadherin-mediated adhesion. *Proc Natl Acad Sci USA* 106: 11594–11599, 2009.
36. **Kee YS, Robinson DN.** Micropipette aspiration for studying cellular mechanosensory responses and mechanics. *Methods Mol Biol* 983: 367–382, 2013.
37. **Kim JB, Islam S, Kim YJ, Prudoff RS, Sass KM, Wheelock MJ, Johnson KR.** N-Cadherin extracellular repeat 4 mediates epithelial to mesenchymal transition and increased motility. *J Cell Biol* 151: 1193–1206, 2000.
38. **Kim NG, Koh E, Chen X, Gumbiner BM.** E-cadherin mediates contact inhibition of proliferation through Hippo signaling-pathway components. *Proc Natl Acad Sci USA* 108: 11930–11935, 2011.
39. **Koenderink GH, Dogic Z, Nakamura F, Bendix PM, MacKintosh FC, Hartwig JH, Stossel TP, Weitz DA.** An active biopolymer network controlled by molecular motors. *Proc Natl Acad Sci USA* 106: 15192–15197, 2009.
40. **Kovacs M, Wang F, Hu A, Zhang Y, Sellers JR.** Functional divergence of human cytoplasmic myosin II: kinetic characterization of the non-muscle IIA isoform. *J Biol Chem* 278: 38132–38140, 2003.
41. **Kreamer BL, Staecker JL, Sawada N, Sattler GL, Hsia MT, Pitot HC.** Use of a low-speed, iso-density percoll centrifugation method to increase the viability of isolated rat hepatocyte preparations. *In Vitro Cell Dev Biol* 22: 201–211, 1986.
42. **Krendel M, Gloushankova NA, Bonder EM, Feder HH, Vasiliev JM, Gelfand IM.** Myosin-dependent contractile activity of the actin cytoskeleton modulates the spatial organization of cell-cell contacts in cultured epitheliocytes. *Proc Natl Acad Sci USA* 96: 9666–9670, 1999.
43. **Lallemand D, Curto M, Saotome I, Giovannini M, McClatchey AI.** NF2 deficiency promotes tumorigenesis and metastasis by destabilizing adherens junctions. *Genes Dev* 17: 1090–1100, 2003.
44. **Liu-Chittenden Y, Huang B, Shim JS, Chen Q, Lee SJ, Anders RA, Liu JO, Pan D.** Genetic and pharmacological disruption of the TEAD-YAP complex suppresses the oncogenic activity of YAP. *Genes Dev* 26: 1300–1305, 2012.
45. **McLaughlin ME, Kruger GM, Slocum KL, Crowley D, Michaud NA, Huang J, Magendantz M, Jacks T.** The Nf2 tumor suppressor regulates cell-cell adhesion during tissue fusion. *Proc Natl Acad Sci USA* 104: 3261–3266, 2007.
46. **Mo JS, Meng Z, Kim YC, Park HW, Hansen CG, Kim S, Lim DS, Guan KL.** Cellular energy stress induces AMPK-mediated regulation of YAP and the Hippo pathway. *Nat Cell Biol* 17: 500–510, 2015.
47. **Olson MF.** Applications for ROCK kinase inhibition. *Curr Opin Cell Biol* 20: 242–248, 2008.
48. **Pan D.** The hippo signaling pathway in development and cancer. *Dev Cell* 19: 491–505, 2010.
49. **Ramaekers FC, Bosman FT.** The cytoskeleton and disease. *J Pathol* 204: 351–354, 2004.
50. **Reginensi A, Scott RP, Gregorieff A, Bagherie-Lachidan M, Chung C, Lim DS, Pawson T, Wrana J, McNeill H.** Yap- and Cdc42-dependent nephrogenesis and morphogenesis during mouse kidney development. *PLoS Genet* 9: e1003380, 2013.
51. **Reichl EM, Ren Y, Morphew MK, Delannoy M, Effler JC, Girard KD, Divi S, Iglesias PA, Kuo SC, Robinson DN.** Interactions between myosin and actin crosslinkers control cytokinesis contractility dynamics and mechanics. *Curr Biol* 18: 471–480, 2008.
52. **Robinson DN, Kee YS, Luo T, Surcel A.** Understanding how dividing cells change shape. In: *Comprehensive Biophysics*, edited by Egelman EH. Oxford: Academic, 2012, p. 48–72.
53. **Sansores-Garcia L, Bossuyt W, Wada K, Yonemura S, Tao C, Sasaki H, Halder G.** Modulating F-actin organization induces organ growth by affecting the Hippo pathway. *EMBO J* 30: 2325–2335, 2011.
54. **Shewan AM, Maddugoda M, Kraemer A, Stehbens SJ, Verma S, Kovacs EM, Yap AS.** Myosin 2 is a key Rho kinase target necessary for the local concentration of E-cadherin at cell-cell contacts. *Mol Biol Cell* 16: 4531–4542, 2005.
55. **Shewan AM, Maddugoda M, Kraemer A, Stehbens SJ, Verma S, Kovacs EM, Yap AS.** Myosin 2 is a key Rho kinase target necessary for the local concentration of E-cadherin at cell-cell contacts. *Mol Biol Cell* 16: 4531–4542, 2005.
56. **Smith AS, Sackmann E.** Progress in mimetic studies of cell adhesion and the mechanosensing. *Chemphyschem* 10: 66–78, 2009.
57. **Somlyo AP, Somlyo AV.** Ca^{2+} sensitivity of smooth muscle and non-muscle myosin II: modulated by G proteins, kinases, and myosin phosphatase. *Physiol Rev* 83: 1325–1358, 2003.
58. **Tojkander S, Gateva G, Lappalainen P.** Actin stress fibers–assembly, dynamics and biological roles. *J Cell Sci* 125: 1855–1864, 2012.
59. **Tremblay AM, Missiaglia E, Galli GG, Hettmer S, Urcia R, Carrara M, Judson RN, Thway K, Nadal G, Selfe JL, Murray G, Calogero RA, De Bari C, Zammit PS, Delorenzi M, Wagers AJ, Shipley J, Wackerhage H, Camargo FD.** The Hippo transducer YAP1 transforms activated satellite cells and is a potent effector of embryonal rhabdomyosarcoma formation. *Cancer Cell* 26: 273–287, 2014.
60. **Vaezi A, Bauer C, Vasioukhin V, Fuchs E.** Actin cable dynamics and Rho/Rock orchestrate a polarized cytoskeletal architecture in the early steps of assembling a stratified epithelium. *Dev Cell* 3: 367–381, 2002.
61. **Vianay B, Kafer J, Planus E, Block M, Graner F, Guillou H.** Single cells spreading on a protein lattice adopt an energy minimizing shape. *Phys Rev Lett* 105: 128101, 2010.

62. **Wang W, Xiao ZD, Li X, Aziz KE, Gan B, Johnson RL, Chen J.** AMPK modulates Hippo pathway activity to regulate energy homeostasis. *Nat Cell Biol* 17: 490–499, 2015.
63. **Wu SK, Gomez GA, Michael M, Verma S, Cox HL, Lefevre JG, Parton RG, Hamilton NA, Neufeld Z, Yap AS.** Cortical F-actin stabilization generates apical-lateral patterns of junctional contractility that integrate cells into epithelia. *Nat Cell Biol* 16: 167–178, 2014.
64. **Yonemura S, Itoh M, Nagafuchi A, Tsukita S.** Cell-to-cell adherens junction formation and actin filament organization: similarities and differences between non-polarized fibroblasts and polarized epithelial cells. *J Cell Sci* 108: 127–142, 1995.
65. **Zhang N, Bai H, David KK, Dong J, Zheng Y, Cai J, Giovannini M, Liu P, Anders RA, Pan D.** The Merlin/NF2 tumor suppressor functions through the YAP oncoprotein to regulate tissue homeostasis in mammals. *Dev Cell* 19: 27–38, 2010.
66. **Zhao B, Li L, Lei Q, Guan KL.** The Hippo-YAP pathway in organ size control and tumorigenesis: an updated version. *Genes Dev* 24: 862–874, 2010.
67. **Zhao B, Ye X, Yu J, Li L, Li W, Li S, Yu J, Lin JD, Wang CY, Chinnaiyan AM, Lai ZC, Guan KL.** TEAD mediates YAP-dependent gene induction and growth control. *Genes Dev* 22: 1962–1971, 2008.